



# Instabilities in shear and simple shear deformations of gold crystals

A.A. Pacheco, R.C. Batra \*

Department of Engineering Science & Mechanics, Virginia Polytechnic Institute & State University, Blacksburg, VA 24061, USA

## ARTICLE INFO

### Article history:

Received 18 May 2008

Received in revised form

4 August 2008

Accepted 14 August 2008

### Keywords:

Local instability criteria

Global instability

Shear and simple shear tests

Average stress and strain tensors

## ABSTRACT

We use the tight-binding potential and molecular mechanics simulations to study local and global instabilities in shear and simple shear deformations of three initially defect-free finite cubes of gold single crystal containing 3480, 7813, and 58,825 atoms. Displacements on all bounding surfaces are prescribed while studying simple shear deformations, but displacements on only two opposite surfaces are assigned during simulations of shear deformations with the remaining four surfaces kept free of external forces. The criteria used to delineate local instabilities in the system include the following: (i) a component of the second-order spatial gradients of the displacement field having large values relative to its average value in the body, (ii) the minimum eigenvalue of the Hessian of the energy of an atom becoming non-positive, and (iii) structural changes represented by a high value of the common neighborhood parameter. It is found that these criteria are met essentially simultaneously at the same atomic position. Effects of free surfaces are evidenced by different deformation patterns for the same specimen deformed in shear and simple shear. The shear strength of a specimen deformed in simple shear is more than three times that of the same specimen deformed in shear. It is found that for each cubic specimen deformed in simple shear the evolution with the shear strain of the average shear stress, prior to the onset of instabilities, is almost identical to that in an equivalent hyperelastic material with strain energy density derived from the tight-binding potential and the assumption that it obeys the Cauchy–Born rule. Even though the material response of the hyperelastic body predicted from the strain energy density is stable over the range of the shear strain simulated in this work, the molecular mechanics simulations predict local and global instabilities in the three specimens.

© 2008 Elsevier Ltd. All rights reserved.

## 1. Introduction

Atomistic simulations improve our understanding of the material response to applied loads, help engineer new alloys or compounds, and may reveal additional physics to be incorporated in phenomenological models of material behavior. Several challenging issues such as the delineation of regions containing dislocations, stacking faults, point defects, and grain boundaries arise during these studies. Here, we focus on studying the initiation of local and global instabilities in an atomic system, and on determining the corresponding deformation measures.

In a homogeneous continuous body, a strong singularity is associated with either the deformation gradient or the displacement becoming discontinuous across a surface passing through a point; e.g., see Truesdell and Noll (1992). The singularity is called weak when both displacements and their first-order derivatives are continuous everywhere in the body

\* Corresponding author. Tel.: +1 540 231 6051; fax: +1 540 231 4574.

E-mail address: [rbatra@vt.edu](mailto:rbatra@vt.edu) (R.C. Batra).

but a second- or a higher-order derivative of the displacement is discontinuous at one or more points of the body. The initiation of a weak singularity at a point is synonymous with an acceleration wave not propagating through that point (Hill, 1962). This is equivalent to the acoustic tensor evaluated at that point having a zero eigenvalue or equivalently a null determinant. van Vliet et al. (2003) and Steinmann et al. (2007), amongst others, have used it to characterize local instabilities in an atomic system.

The potential energy of a system of atoms is usually assumed to depend upon the current inter-atomic distances and the relative angles between atomic bonds. From a continuum point of view, this is equivalent to assuming that an appropriately defined strain energy density depends upon the state of deformation in the present configuration, or equivalently, the material response is elastic. The material objectivity is satisfied since inter-atomic distances and the changes in angles between atomic bonds are invariant with respect to superimposed rigid body motions.

The implementation of continuum concepts such as the acoustic tensor becoming singular at the onset of a local instability is equivalent to assuming that the matrix of instantaneous values of elasticities, defined as the second-order derivatives of the strain energy density with respect to the Green–St. Venant strain tensor, ceases to be positive definite. In the phonon theory the acoustic tensor is called the dynamical matrix and is basically discrete. However, in continuum mechanics the acoustic tensor is defined at every point in the continuum and is a continuous function of the deformation gradient. For discrete systems Lu and Zhang (2006) have used an atomistic counterpart of the continuum acoustic tensor called the atomic acoustic tensor to study the nucleation of local instabilities. It is equivalent to requiring that the energy of every atom in the system in equilibrium be convex for variations of position vectors of other atoms given by a mono-mode perturbation.

The configuration of a system in equilibrium is globally stable if its potential energy in that configuration is the minimum. Kitamura et al. (2004a) studied delamination of a nano-film from a substrate and found that the displacement at which the minimum eigenvalue of the Hessian of the potential energy of the system vanished equaled that at which the load–displacement curve became discontinuous (the displacement abruptly increased under the applied load). The same criterion has been used to analyze strengths of thin films and cracked bodies (Kitamura et al., 2004b).

Instabilities in an atomic system have been studied also by the normal mode analysis (Dimitriev et al., 2005) which exploits symmetries of the system to reduce the number of degrees of freedom (d.o.f.). For a system having no spatial symmetries, the normal mode analysis is equivalent to the method used by Kitamura et al. (2004a, b). For a system having no symmetries, the reduction of the number of d.o.f. is not possible. The implementation of a criterion which includes all d.o.f. is prohibitive for a large system because of difficulties in finding an eigenvalue of a  $3N_a \times 3N_a$  sparse matrix where  $N_a$  is the number of d.o.f. after the elimination of all prescribed displacements. Moreover, modal analysis shows not only instabilities related to the constituent material but also structural instabilities that are influenced by the magnitude of external loads and the type of constraints. Thus a local criterion helps characterize material instabilities, and determine the permissible loading capacity of a system.

Regions where deformations of an atomic system first become unstable have also been identified by using geometric measures of the local atomic structure. For example, for an FCC crystal Kelchner et al. (1998) used the centrosymmetry parameter that measures the relative positions between six pairs of nearest atoms situated on opposite sides of the atom whose centrosymmetric parameter is being calculated. Other quantities used include the slip vector (Zimmerman et al., 2001), the atomic bond rotation angle (Li and Li, 2006), the common neighborhood parameter (CNP) (Tsuzuki et al., 2007), and invariants of the infinitesimal strain tensor (Pasianot et al., 1993). Hartley and Mishin (2005) computed the local deformation gradient by employing the least-squares method (LSM) and the Cauchy–Born rule, and used contour plots of components of the Nye tensor to identify screw and edge dislocations in a system of copper atoms. Since the integration of the Nye tensor over an area enclosed by Burger's circuit equals the Burger vector, Hartley and Mishin (2005) asserted that this technique identifies well dislocations. Zimmerman et al. (2001) used the slip vector for identifying dislocations and finding an approximation of Burger's vector.

Here we use the tight-binding (TB) potential and molecular mechanics (MM) simulations to study shear and simple shear deformations of a system of gold (Au) atoms, and use (i) second-order gradients of the displacement field, (ii) the CNP (Tsuzuki et al., 2007), (iii) eigenvalues of the local acoustic tensor, and (iv) eigenvalues of the Hessian of the local potential energy to characterize the onset of local instabilities. We also investigate whether or not these four criteria are met simultaneously at a point. We find the local Hessian of the TB potential by considering the bond energy between an atom and other atoms included in the first shell of neighbors. The first shell of neighbors contains atoms located within one atomic spacing of the atom whose stability is being investigated. In the physics literature, MM simulations are usually referred to as the molecular static simulations.

Values of the first- and the second-order displacement gradients are found by using the modified smoothed particle hydrodynamics (MSPH) method (Zhang and Batra, 2004). Values of the average Cauchy stress tensor for each system are computed by using four definitions of the average stress tensor. Average stresses and strains for the simple shear deformations are also compared with those deduced by assuming that the Cauchy–Born rule applies and the response of the atomic system is equivalent to that of a simple hyperelastic body with the strain energy density equal to that given by the TB potential. However, the Cauchy–Born rule is used till the onset of a global instability.

The global instability of the system is characterized either by a sharp discontinuity in the average shear stress—average shear strain curve or the potential energy of the system ceasing to be the minimum.

The rest of the paper is organized as follows. The TB potential is summarized in Section 2 where we also describe how numerical simulations are conducted. Measures of the average stresses and strains are delineated in Section 3 where we

provide details of the MSPH method used to compute displacement gradients at a point. The strain energy density of a simple hyperelastic material equivalent to the Au crystal defined by the TB potential is derived in Section 3.3. Section 4 describes the shear test and the simple shear test. In Section 5 we present and discuss results of average stresses and strains for the two shear tests. The criteria for the local and the global instabilities are described in Section 6. These are used to characterize instabilities in shear and simple shear deformations of Au crystals. Conclusions of the work are summarized in Section 7.

## 2. Molecular mechanics simulations

### 2.1. Molecular mechanics (MM) potential

We use the TB potential

$$V^{(i)} = - \left( \sum_{\substack{j=1 \\ j \neq i}}^N \zeta^2 \exp \left( -2D \left( \frac{r^{(ij)}}{r_0} - 1 \right) \right) \right)^{1/2} + \sum_{\substack{j=1 \\ j \neq i}}^N M \exp \left( -\tilde{P} \left( \frac{r^{(ij)}}{r_0} - 1 \right) \right) \quad (1)$$

proposed by Cleri and Rosato (1993) to describe interactions among atoms. In Eq. (1)  $N$  equals the total number of atoms in the system,  $r_0$  the first-neighbor distance ( $a/\sqrt{2}$ , where  $a$  is the lattice parameter),  $r^{(ij)}$  is the magnitude of the position vector between atoms  $i$  and  $j$ , and  $\zeta$ ,  $D$ ,  $\tilde{P}$ , and  $M$  are constants characterizing a material. Values of material parameters for Au are (Cleri and Rosato, 1993)

$$M = 0.2061 \text{ eV}, \quad \zeta = 1.7900 \text{ eV}, \quad \tilde{P} = 10.229, \quad D = 4.0360, \quad r_0 = 2.8850 \text{ \AA}.$$

This potential has been used successfully to characterize the mechanical behavior of Au nanowires (Ju et al., 2004; Lee et al., 2006, Lin et al., 2005). Pu et al. (2007) used three semi-empirical potentials, namely, the Voter and Chen's (1987) embedded atomic method (EAM) potential, the glue model potential of Ercolessi et al. (1998), and the TB potential (1). They compared results of MD simulations for a tension test on an Au cluster composed of 256 atoms using three different potentials, namely the glue model, the TB potential, and the EAM potential. The predictive capability of each inter-atomic potential was determined by comparing its predictions of the potential energy in the relaxed configuration and the ultimate force at the breaking point with the results obtained by using the Density Functional Theory (DFT) which were taken as the reference values. The force at the breaking point for an atomic chain of Au atoms was also found experimentally by Rubio-Bollinger et al. (2001) to be  $1.5 \pm 0.3$  nN. The results given by the TB potential of Cleri and Rosato were found to agree well with the DFT results and the experimental data.

Since  $V^{(i)}$  is essentially zero for  $r^{(ij)} > 5.5 \text{ \AA}$ , the summation in Eq. (1) is carried out only for those values of  $j$  for which  $r^{(ij)} < 6 \text{ \AA}$  to reduce the computational cost. Thus only atoms lying within a distance of  $6 \text{ \AA}$  from the atom  $i$  contribute to the potential energy of atom  $i$ . We note that the TB potential and its first derivatives are continuous at the cut off radius of  $6 \text{ \AA}$  within the accuracy of the machine.

The internal energy  $V$  of the system equals the sum of the energy  $V^{(i)}$  of all atoms in the system. That is

$$V = \sum_{i=1}^N V^{(i)}(r^{(ij)}). \quad (2)$$

The interaction force vector  $\mathbf{f}^{(ij)}$  between atoms  $i$  and  $j$  equals the negative of the gradient of the internal energy with respect to components of the relative position vector  $\mathbf{r}^{(ij)}$ , or

$$f_{\alpha}^{(ij)} = - \left( \frac{\partial V^{(i)}}{\partial r^{(ij)}} + \frac{\partial V^{(j)}}{\partial r^{(ji)}} \right) \frac{r_{\alpha}^{(ij)}}{r^{(ij)}}. \quad (3)$$

Here and below, the index  $\alpha$  ranges from 1 to 3, and  $f_{\alpha}^{(ij)}$  equals the component of  $\mathbf{f}^{(ij)}$  along the  $x_{\alpha}$ -coordinate direction of a rectangular Cartesian coordinate system.

### 2.2. Description of a numerical simulation

We study static deformations at 0K, and start the numerical simulation by assigning the initial position vector  $\mathbf{X}^{(i)}$  of each atom in the system in a perfect lattice configuration (cf. Fig. 1). Each atom is allowed to move freely till the potential energy of the system has been minimized by using the conjugate gradient with warranted descent technique of Hager and Zhang (2005). The minimization procedure is stopped when the magnitude of each component of the gradient of the internal energy at every atom in the system equals at most  $1 \times 10^{-8}$  eV/Å. The position vector of an atom in this relaxed configuration is denoted by  $\mathbf{X}_R^{(i)}$ , and this configuration is called the reference configuration. This is equivalent to annealing a specimen before conducting a mechanical test. Subsequently, after each increment in the prescribed displacements of atoms on the bounding surfaces of the body, the total potential energy is minimized, i.e., the system is allowed to

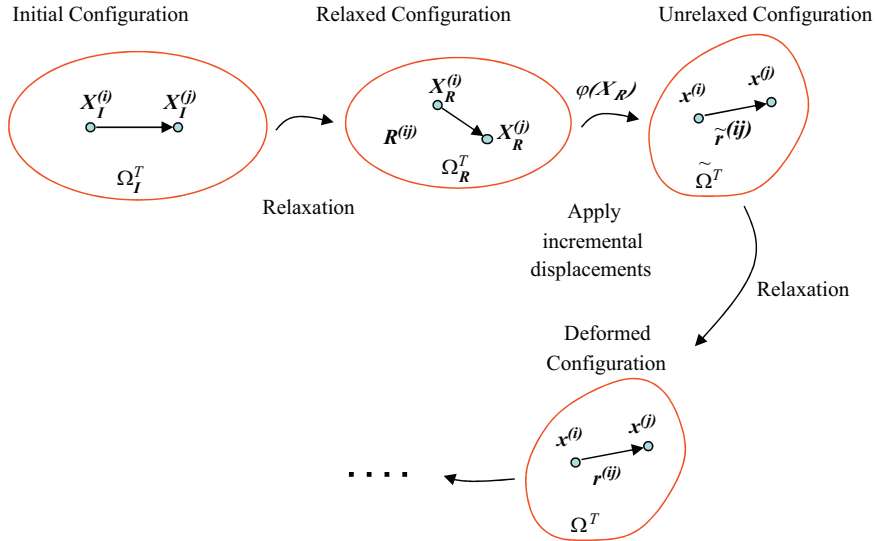


Fig. 1. Schematics of the initial, the relaxed (reference), and the current (deformed) configurations of an atomic system.

equilibrate after every load step. The change in the potential energy of the system from that in the reference configuration equals the strain energy required to deform the body or the system of atoms. The process is continued till atoms on the bounding surface have been displaced by the prescribed amount.

In problems studied here, either an atom on the bounding surface has a displacement component prescribed or the corresponding traction component is null in the sense that there is no external force applied at that atom.

### 3. Determination of macroscopic variables

#### 3.1. Strains

Mott et al. (1992) studied 3D deformations of an atomic system, and interpolated displacements using a continuous, piecewise-linear basis functions formed by a Delaunay tessellation of the atomic positions. Falk (1999) computed infinitesimal strains based on the relative displacements between two neighboring atoms. Webb et al. (2008) have also computed displacement gradients from atomic positions.

We employ the MSPH method (Zhang and Batra, 2004) to compute the spatial distribution of the deformation gradient  $\mathbf{F}$  and the second-order gradients  $\mathbf{G}$  of displacements from positions of atoms in the current and the reference configurations. The Cauchy–Born rule (Stakgold, 1950; Born and Huang, 1954; Ericksen, 2008, and references cited therein) states that for a crystal with a simple Bravais lattice, relative position vectors  $\mathbf{r}^{(ij)}$  and  $\mathbf{R}^{(ij)}$  between atoms  $i$  and  $j$  in the current and the reference configurations are related by  $\mathbf{r}^{(ij)} = \mathbf{F}^{(i)} \mathbf{R}^{(ij)}$  where  $\mathbf{F}^{(i)}$  is the deformation gradient at the position of atom  $i$  in the reference configuration. To partially account for non-local interactions in continuum mechanics, Kouznetsova et al. (2002) also considered  $\mathbf{G}$  in the kinematic description of the deformation. We propose to use components of the tensor  $\mathbf{G}$  to characterize local instabilities in an atomic system (cf. Section 6).

In the MSPH method it is assumed that a function  $\varphi(\mathbf{X})$  (e.g., the position vector component  $r_x^{(i)}$ ) has continuous derivatives up to  $(n+1)$ th order. The three-term Taylor series expansion of  $\varphi(\mathbf{X})$  at the point  $\xi = (\xi_1, \xi_2, \xi_3)$  in the neighborhood of the point  $\mathbf{X} = \mathbf{X}^{(i)} = (X_1^{(i)}, X_2^{(i)}, X_3^{(i)})$  is

$$\varphi(\xi) = \varphi(\mathbf{X}^{(i)}) + \frac{\partial \varphi}{\partial X_\alpha^{(i)}} (\xi_\alpha - X_\alpha^{(i)}) + \frac{1}{2} \frac{\partial^2 \varphi}{\partial X_\alpha^{(i)} \partial X_\beta^{(i)}} (\xi_\alpha - X_\alpha^{(i)}) (\xi_\beta - X_\beta^{(i)}), \quad (4)$$

where summation on repeated Greek indices is implied, and  $\partial \varphi / \partial X_\alpha^{(i)} = \partial \varphi / \partial X_\alpha |_{\mathbf{X}=\mathbf{X}^{(i)}}$ . To evaluate the function  $\varphi(\mathbf{X})$  and its first- and second-order derivatives at the point  $\mathbf{X}^{(i)}$ , we multiply both sides of Eq. (4) with a non-negative kernel function  $W(|\mathbf{X}-\xi|, h)$  of compact support, and by its first- and second-order derivatives,  $W_{,\alpha}(|\mathbf{X}-\xi|, h)$  and  $W_{,\alpha\beta}(|\mathbf{X}-\xi|, h)$ ; here  $W_{,\alpha} = \partial W / \partial \xi_\alpha$  and  $W_{,\alpha\beta} = \partial^2 W / \partial \xi_\alpha \partial \xi_\beta$ , and  $h$  is the smoothing length which determines the size of the compact support of the kernel function  $W$ . The magnitude of  $h$  usually equals three times the atomic spacing. For a three-dimensional (3D) problem one needs at least ten atoms within the compact support of  $W(|\mathbf{X}-\xi|, h)$ . We integrate the resulting equations with respect to  $\xi$  over the volume  $\Omega_K^T$  occupied by the system in the relaxed configuration, employ atomic positions as integration points, and volumes associated with them as the corresponding weights to obtain a set of ten algebraic equations for  $\varphi(\mathbf{X})$ ,  $\varphi_{,\alpha}(\mathbf{X})$ , and  $\varphi_{,\alpha\beta}(\mathbf{X})$ . Setting  $\varphi(\mathbf{X}) = r_x^{(i)}$  gives values of  $\mathbf{F}$  and  $\mathbf{G}$  at the point  $\mathbf{X}$ . Unless the function

$W(|\mathbf{X}-\xi|,h)$  is a constant over its compact support, the influence of displacements of atom  $j$  on values of  $\mathbf{F}$  and  $\mathbf{G}$  at the point  $\mathbf{X}^{(i)}$  occupied by atom  $i$  depends upon the relative values of  $W(|\mathbf{X}-\xi|,h)$  at locations of atoms  $i$  and  $j$ . For a 3D problem, one needs to solve three systems of ten simultaneous linear algebraic equations to find displacements, and  $\mathbf{F}$  and  $\mathbf{G}$  at a point.

We use the following cubic spline kernel function  $W$ :

$$W(s) = \frac{1}{\pi h^3} \begin{cases} \left(1 - \frac{3}{2}s^2 + \frac{3}{4}s^3\right), & s \leq 1, \\ \frac{1}{4}(2-s)^3, & 1 < s \leq 2, \\ 0, & \text{otherwise,} \end{cases} \quad (5)$$

$$s = \frac{\|\mathbf{X} - \xi\|}{h} = \frac{r}{h}. \quad (6)$$

Other techniques like the LSM or the LSM in conjunction with smoothing functions (Gullett et al., 2008) can also be used to find values of  $\mathbf{F}^{(i)}$  at the location of atom  $i$ .

From  $\mathbf{F}^{(i)}$  at the point  $\mathbf{x}^{(i)}$ , we evaluate there the Almansi–Hamel strain tensor  $\mathbf{e}^{(i)}$  from

$$e_{\alpha\beta}^{(i)} = (1/2)(\delta_{\alpha\beta} - (F^{-1})_{\phi\alpha}^{(i)}(F^{-1})_{\phi\beta}^{(i)}),$$

where  $\delta_{\alpha\beta}$  is the Kronecker delta. The volume averaged value,  $\bar{\mathbf{e}}$ , of this tensor for the system is defined by

$$\bar{e}_{\alpha\beta} = \frac{1}{\Omega^T} \int_{\Omega} e_{\alpha\beta}(\mathbf{x}) \, d\Omega = \sum_{i=1}^N \frac{\Omega^{(i)}}{\Omega^T} e_{\alpha\beta}^{(i)}, \quad (8)$$

where  $\Omega^{(i)}$  and  $\Omega^T$  equal, respectively, the volume assigned to atom  $i$  and the total volume of the system in the deformed configuration. We set  $\Omega^{(i)}$  equal to the Voronoi volume associated with atom  $i$ . An approximation of the Voronoi volume is given by (e.g., see Lin et al., 2005)

$$\Omega^{(i)} = \frac{4\pi}{3} a_i^3, \quad a_i = k_v \frac{\sum_{j=1}^{N_e} (r^{(ij)})^{-1}}{\sum_{j=1}^{N_e} (r^{(ij)})^{-2}}. \quad (9)$$

Here  $N_e$  equals the number of atoms in the neighborhood of atom  $i$  for which  $r^{(ij)} \leq (\sqrt{3}/2)a$ , and we set the constant  $k_v = 0.55$ . The value of  $k_v$  was found by computing the Voronoi volume of an atom at the centroid of the specimen, and equating it to the volume given by Eq. (9).

### 3.2. Stresses

For a system comprised of  $N$  atoms, the average values  $\bar{\sigma}_{\alpha\beta}$  of components of the Cauchy stress tensor are computed by considering all atoms in the system and by using the relation

$$\bar{\sigma}_{\alpha\beta} = \frac{1}{2\Omega^T} \sum_{i=1}^N \sum_{\substack{j=1 \\ j \neq i}}^N f_{\alpha}^{(ij)} r_{\beta}^{(ij)}. \quad (10)$$

That is,  $\bar{\sigma}_{\alpha\beta}$  equals the average value of the corresponding component of the configurational part of the virial stress tensor (Cornier et al., 2001).

The average value over volume  $\Omega$  of the Cauchy stress tensor defined by

$$\bar{\sigma}_{\alpha\beta} = \frac{1}{\Omega} \int_{\Omega} \sigma_{\alpha\beta} \, d\Omega \quad (11)$$

can be written as

$$\begin{aligned} \bar{\sigma}_{\alpha\beta} &= \frac{1}{\Omega} \int_{\Omega} \sigma_{\alpha\phi} \delta_{\phi\beta} \, d\Omega = \frac{1}{\Omega} \int_{\Omega} \sigma_{\alpha\phi} x_{\beta,\phi} \, d\Omega, \\ &= \frac{1}{\Omega} \int_{\Omega} (\sigma_{\alpha\phi} x_{\beta})_{,\phi} \, d\Omega - \frac{1}{\Omega} \int_{\Omega} \sigma_{\alpha\phi,\phi} x_{\beta} \, d\Omega, \end{aligned} \quad (12)$$

where  $x_{\beta,\phi} = \partial x_{\beta} / \partial x_{\phi} = \delta_{\beta\phi}$ . Using the divergence theorem on the first term on the right-hand side of Eq. (12), and the balance of linear momentum with null body forces, we get

$$\begin{aligned} \bar{\sigma}_{\alpha\beta} &= \frac{1}{\Omega} \int_{\partial\Omega} \sigma_{\alpha\phi} x_{\beta} n_{\phi} \, dS, \\ &= \frac{1}{\Omega} \int_{\partial\Omega} t_{\alpha} x_{\beta} \, dS, \end{aligned} \quad (13)$$

where  $\mathbf{n}$  is a unit outward normal to the boundary  $\partial\Omega$  of  $\Omega$ , and  $\mathbf{t} = \boldsymbol{\sigma}\mathbf{n}$  is the surface traction. Thus the average Cauchy stress tensor multiplied by the volume of the region equals the first moment of tractions acting on the bounding surface of the body.

For a discrete system, Eq. (13) can be written as

$$\bar{\sigma}_{\alpha\beta} = \frac{1}{\Omega^T} \sum_{i=1}^{N_b} x_{\beta}^{(i)} f_{\alpha}^{(i)}, \quad (14)$$

where  $N_b$  equals the number of atoms on the bounding surface of the region whose deformations are being studied.

Assuming that the volume assigned to each atom is the same, Eq. (10) becomes

$$\bar{\sigma}_{\alpha\beta} = \frac{1}{N} \sum_{i=1}^N \frac{1}{2\Omega^{(i)}} \sum_{\substack{j=1 \\ j \neq i}}^N f_{\alpha}^{(ij)} r_{\beta}^{(ij)} = \frac{1}{N} \sum_{i=1}^N \omega_{\alpha\beta}^{(i)}, \quad (15)$$

where  $\omega_{\alpha\beta}^{(i)}$  is identified as the dipole force tensor (Potirniche et al., 2006). However, for a finite size specimen, Eq. (15) is approximately valid since the volume assigned to an atom on the bounding surface equals 1/2 of that assigned to an atom in the interior of the body. Also, the volume of an atom at a vertex is taken to equal 1/8 of that for an interior atom.

### 3.3. Stress and strain tensors for simple shearing deformations

Consider a system of atoms with a simple Bravais lattice deformed homogeneously by the deformation gradient

$$[F(k_s)] = \begin{bmatrix} 1 & k_s & 0 \\ 0 & 1 & 0 \\ 0 & 0 & 1 \end{bmatrix}, \quad (16.1)$$

for which

$$[\varepsilon(k_s)] = \begin{bmatrix} 0 & k_s/2 & 0 \\ k_s/2 & k_s^2/2 & 0 \\ 0 & 0 & 0 \end{bmatrix}, \quad (16.2)$$

where  $k_s$  is a positive constant. Assuming that the overall response of the system of atoms is equivalent to that of a simple hyperelastic body with the strain energy density  $W_0$  defined by

$$W_0(\mathbf{F}) = \sum_i^N \frac{V^{(i)}}{\Omega_R^{(i)}}, \quad (17)$$

where  $\Omega_R^{(i)}$  is the volume associated with atom  $i$  in the reference configuration, and  $\sum_{i=1}^N \Omega_R^{(i)} = \Omega_R^T$ , the volume occupied by the body in the reference configuration. The first Piola–Kirchhoff stress tensor  $\bar{\mathbf{P}}$  is given by

$$\bar{\mathbf{P}} = \frac{\partial W_0}{\partial \mathbf{F}} = \frac{\partial}{\partial \mathbf{F}} \left( \sum_{i=1}^N \frac{V^{(i)}}{\Omega_R^{(i)}} \right) \quad (18)$$

or equivalently by

$$\bar{P}_{\alpha\beta} = \sum_{i=1}^N \sum_{\substack{k=1 \\ k \neq i}}^N \frac{1}{\Omega_R^{(i)}} \frac{\partial V^{(i)}}{\partial r^{(ik)}} \frac{\partial r^{(ik)}}{\partial r_{\gamma}^{(ik)}} \frac{\partial r_{\gamma}^{(ik)}}{\partial F_{\alpha\beta}} = \sum_{\substack{k=1 \\ i \neq k}}^N \frac{1}{\Omega_R^{(i)}} \frac{1}{r^{(ik)}} \frac{\partial V^{(i)}}{\partial r^{(ik)}} r_{\alpha}^{(ik)} R_{\beta}^{(ik)}. \quad (19)$$

For simple shear deformations, we get

$$[\bar{\mathbf{P}}(k_s)] = \sum_{\substack{k=1 \\ i \neq k}}^N \frac{1}{\Omega_R^{(i)}} \frac{1}{r^{(ik)}} \frac{\partial V^{(i)}}{\partial r^{(ik)}} [\Phi^{(ik)}(k_s)], \quad (20)$$

where

$$[\Phi^{(ik)}(k_s)] = \begin{bmatrix} R_{xx}^{(ik)} + k_s R_{xy}^{(ik)} & R_{xy}^{(ik)} + k_s R_{yy}^{(ik)} & R_{xz}^{(ik)} + k_s R_{yz}^{(ik)} \\ R_{yx}^{(ik)} & R_{yy}^{(ik)} & R_{yz}^{(ik)} \\ R_{zx}^{(ik)} & R_{zy}^{(ik)} & R_{zz}^{(ik)} \end{bmatrix},$$

$$(r^{(ik)})^2 = R_{\xi}^{(ik)} R_{\xi}^{(ik)} + 2k_s R_{xy}^{(ik)} + 3k_s^2 (R_y^{(ik)})^2,$$

and  $R_{xy}^{(ik)} = R_x^{(ik)} R_y^{(ik)}$ ,  $R_{yy}^{(ik)} = R_y^{(ik)} R_y^{(ik)}$ , ... From expression (19) of the first Piola–Kirchhoff stress tensor, we obtain the following formula for the Cauchy stress tensor:

$$[\bar{\sigma}(k_s)] = \sum_{\substack{i,k=1 \\ i \neq k}}^N \frac{1}{\Omega^{(i)}} \frac{1}{r^{(ik)}} \frac{\partial V^{(i)}}{\partial r^{(ik)}} [\Theta^{(ik)}(k_s)], \quad (21)$$

where

$$[\Theta^{(ik)}(k_s)] = \begin{bmatrix} R_{xx}^{(ik)} + k_s R_{xy}^{(ik)} + k_s (R_{xy}^{(ik)} + k_s R_{yy}^{(ik)}) & R_{xy}^{(ik)} + k_s R_{yy}^{(ik)} & R_{xz}^{(ik)} + k_s R_{yz}^{(ik)} \\ R_{yx}^{(ik)} + k_s R_{yy}^{(ik)} & R_{yy}^{(ik)} & R_{yz}^{(ik)} \\ R_{zx}^{(ik)} + k_s R_{zy}^{(ik)} & R_{zy}^{(ik)} & R_{zz}^{(ik)} \end{bmatrix}$$

Here we have set  $\Omega^{(i)} = J \Omega_R^{(i)} = \Omega_R^{(i)}$  since  $J = \det[\mathbf{F}] = 1$ . We note that  $r^{(ij)}$  and  $\partial V^{(i)} / \partial r^{(ik)}$  also depend upon  $k_s$ . Thus one cannot characterize the dependence of  $\bar{\sigma}$  upon  $k_s$  simply from the expression for  $[\Theta^{(ik)}(k_s)]$ .

## 4. Simulation of deformations

### 4.1. Shear test

We simulate the shear test on cubic Au crystal specimens of three different sizes. System A with side  $\sim 32 \text{ \AA}$  contains 3480 atoms, system B with side  $\sim 50 \text{ \AA}$  has 7813 atoms, and system C with side  $\sim 100 \text{ \AA}$  has 58,825 atoms. In each case, atoms are located in planes parallel to the coordinate planes  $\{100\}$ ,  $\{010\}$ , and  $\{001\}$ . After finding the initial relaxed configuration, atoms on the bottom surface  $Y = Y_{\min}$  are constrained from moving in all directions. For atoms on the top surface,  $Y = Y_{\max}$ , the  $Y$ - and  $Z$ -displacements are set equal to zero and the  $X$ -displacement is prescribed in increments of  $0.0025 \text{ \AA}$ . The magnitude of the incremental  $X$ -displacement was halved if the potential energy of the deformed configuration could not be minimized in a pre-assigned number of iterations. There are no external surface forces applied on the remaining four bounding faces. A schematic of the problem studied is exhibited in Fig. 2a, in which atoms enclosed in red boxes have prescribed displacements.

### 4.2. Simple shear test

The simulation of the simple shear test (cf. Fig. 2b) differs from that of the shear test described above only in boundary conditions prescribed on the bounding surfaces. In this case, the three components of displacement are prescribed on all bounding surfaces so that  $x = X + k_s Y$ ,  $y = Y$ ,  $z = Z$ , where  $(x, y, z)$  are coordinates of the atom in the deformed configuration that in the reference configuration was located at  $(X, Y, Z)$ . Only interior atoms are allowed to move during the minimization of the potential energy of the system. The non-dimensional constant  $k_s = \tan(\gamma)$  is increased in increments of  $0.0025$  to induce additional deformations of the body.

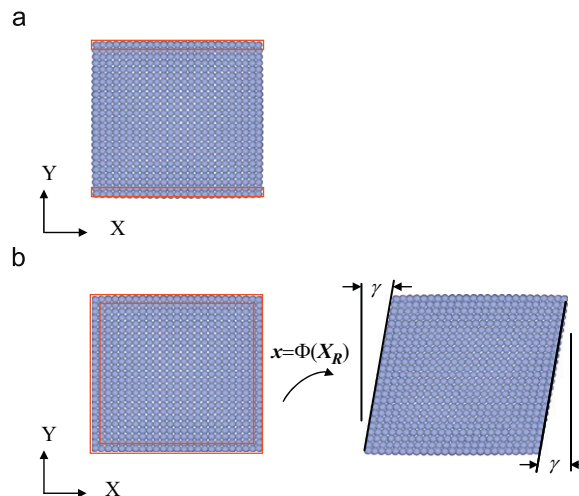


**Fig. 2.** (a) Reference configuration of a gold specimen for the shear test. (b) Reference and deformed configurations of a gold specimen for the simple shear test. Displacements of atoms enclosed in the red boxes are prescribed.

## 5. Average stresses and strains from results of numerical simulations

### 5.1. Shear test

Fig. 3 shows the variation with the shear angle  $\gamma$  of the average components of the Cauchy stress tensor defined by Eqs. (10) and (14). Ideally, the two equations should give the same values of stress components. Results plotted in Fig. 3 for the three systems reveal that, in each case, the shear stress  $\sigma_{xy}$  and the normal stress  $\sigma_{yy}$  are dominant, and their values computed from Eqs. (10) and (14) are nearly equal to each other. Furthermore, the evolution of  $\sigma_{yy}$  with the shear angle  $\gamma$  is qualitatively similar for the three specimens. Recall that the average stress defined by Eq. (14) is computed from forces and positions of atoms at the boundaries. In Table 1 we have listed, for the three specimens, values of the maximum shear stress  $\sigma_{xy}$ , the maximum von Mises stress  $\sigma_{VM}^{\max}$ ,  $\sigma_{xy}$ , and  $\sigma_{VM}$  at yield, and values of the angle  $\gamma$  at the proportionality limit and at the yield point. We note that the von Mises stress defined as  $\sigma_{VM} = (1/\sqrt{2})\sqrt{(\sigma_{11} - \sigma_{22})^2 + (\sigma_{22} - \sigma_{33})^2 + (\sigma_{33} - \sigma_{11})^2 + 6(\sigma_{12}^2 + \sigma_{13}^2 + \sigma_{23}^2)}$ , is proportional to the second invariant of the Cauchy stress tensor. The yielding of the material is identified by a drop in the shear stress with an increase in the shear strain. The variation of  $\sigma_{xy}$  with  $\gamma$  is linear for  $\gamma \leq \gamma_{\text{linear}}$  while values of  $\sigma_{xz}$  and  $\sigma_{yz}$  are negligible as compared to those of  $\sigma_{xy}$  up to  $\gamma = \gamma_{\text{yield}}$  where the first discontinuity in the shear stress vs. the shear angle curve appears. The number of atoms in the system being studied affects significantly values of the yield stress and the yield strain. Because of the scale used to plot results, it is not easy to delineate  $\gamma_{\text{linear}}$  in the stress vs.  $\gamma$  curves. Whereas,  $\gamma_{\text{linear}}$  for specimens B and C differ by  $\sim 6\%$ ,  $\gamma_{\text{yield}}$  for specimen C is nearly 72% of that for specimen B. Similarly, the shear stress at yield and the maximum shear stress for specimen C equal nearly 70% of those for specimen B. Because of the limited computational resources available, larger specimens could not be studied. The simulation of the shear and the simple shear deformations in larger specimens should give fully converged values of the yield stress and the maximum shear stress.

We hypothesize that at  $\gamma = \gamma_{\text{yield}}$  there is a critical density of unstable atoms so that the local atomic structure changes noticeably, dislocations originate, and the body subsequently deforms plastically. Unfortunately, we cannot compute the Burger's vector because at the onset of the global instability the local instability has initiated at nearly 40% of atoms. If we adopt Considère's (1888) criterion according to which a system becomes globally unstable at the peak in the load (or equivalently the shear stress for the problem being studied), then the global and the local instabilities initiate at different values of the shear strain as should be evident from results of specimen C summarized in Table 1 and depicted in Fig. 3e. For this specimen  $\gamma_{\text{yield}} = 0.084$ , and  $\sigma_{xy}^{\max} = 2.408$  GPa occurs at  $\gamma = 0.102$ . For specimen C there are two discontinuities in the shear stress  $\sigma_{xy}$  vs.  $\gamma$  curve, the first corresponding to the yielding of the material and the second corresponding to the global instability discussed in Section 6. However, for specimens A and B only one sharp discontinuity in the  $\sigma_{xy}$  vs.  $\gamma$  curve is observed. Thus whether yielding is followed by the global instability or the two occur simultaneously depends upon the number of atoms in the system studied.

Values of the shear modulus  $C_{44}$ , based on the average shear stress, and obtained by linear regression of the shear stress—the shear angle curve for points up to  $\gamma_{\text{linear}}$ , equal 32.23, 31.08, and 28.26 GPa for systems A, B, and C, respectively. Since  $\gamma_{\text{linear}} \leq 0.044$ ,  $k_s \approx \gamma$ . We note that elastic constants for Au were used to find values of parameters in the TB potential given by Eq. (1). Accordingly, we should have obtained  $C_{44}$  equal to 45 GPa. The difference in the computed and the ideal values of  $C_{44}$  is partly due to changes in lattice parameter at points near bounding surfaces that occur during the relaxation of the initial configuration; cf. Fig. 4a. Only at points close to the centroid of the specimen the lattice parameter  $a$  equals 4.079 Å, that is, the value for a pristine Au crystal. To eliminate the effect of inhomogeneous deformations of atoms near free surfaces, we compute the value of  $C_{44}$  based on the shear stress averaged over a spherical representative volume (SRV) of radius  $R$  around specimen's centroid. From the results plotted in Fig. 4b, it can be observed that for small SRVs computed values of  $C_{44}$  are close to that for a pristine crystal. However, with an increase in the value of  $R$ , the value of the shear modulus saturates to a value of 28.26 GPa.

The evolution of components of the average Almansi–Hamel strain tensor with the shear angle  $\gamma$  is plotted in Fig. 5. For each one of the three systems, and for  $\gamma < \gamma_{\text{yield}}$  the variation of the averaged shear strain component  $\varepsilon_{xy}$  with  $\gamma$  is linear while  $\varepsilon_{xz}$  and  $\varepsilon_{yz}$  are negligibly small. The evolution of the averaged normal strains  $\varepsilon_{yy}$  and  $\varepsilon_{zz}$  for the three specimens is essentially similar, but their magnitudes decrease with an increase in the number of atoms in the system studied. The difference in the maximum values of axial or normal strains from system A to system C is about 40%. Prior to yielding,  $\varepsilon_{yy}$  and  $\varepsilon_{zz}$  are negative but  $\varepsilon_{xx}$  is positive. For specimen C magnitudes of normal strains are approximately an order of magnitude smaller than that of  $\varepsilon_{xy}$ . Subsequent to the system becoming globally unstable, stress components exhibit oscillations with an increase in  $\gamma$ ; reasons for these oscillations are not obvious.

The evolution with the shear angle  $\gamma$  of stresses and strains plotted in Figs. 3 and 5 suggests that for a given value of  $\gamma$ , the shear stress  $\sigma_{xy}$  and the shear strain  $\varepsilon_{xy}$  have higher values than the other two shear stresses and the other two shear strains, respectively. Whereas  $\sigma_{xx}$  and  $\sigma_{zz}$  have negligible values until the discontinuity in the stresses at  $\gamma = \gamma_{\text{yield}}$  appears, the normal stress  $\sigma_{yy}$  is compressive and its magnitude is about 20% of that of the shear stress  $\sigma_{xy}$ . Thus compressive normal tractions need to be applied to the top and the bottom surfaces. In the absence of these normal tractions, the height of the specimen will increase. It confirms the Poynting effect in non-linear elasticity (Poynting, 1909).

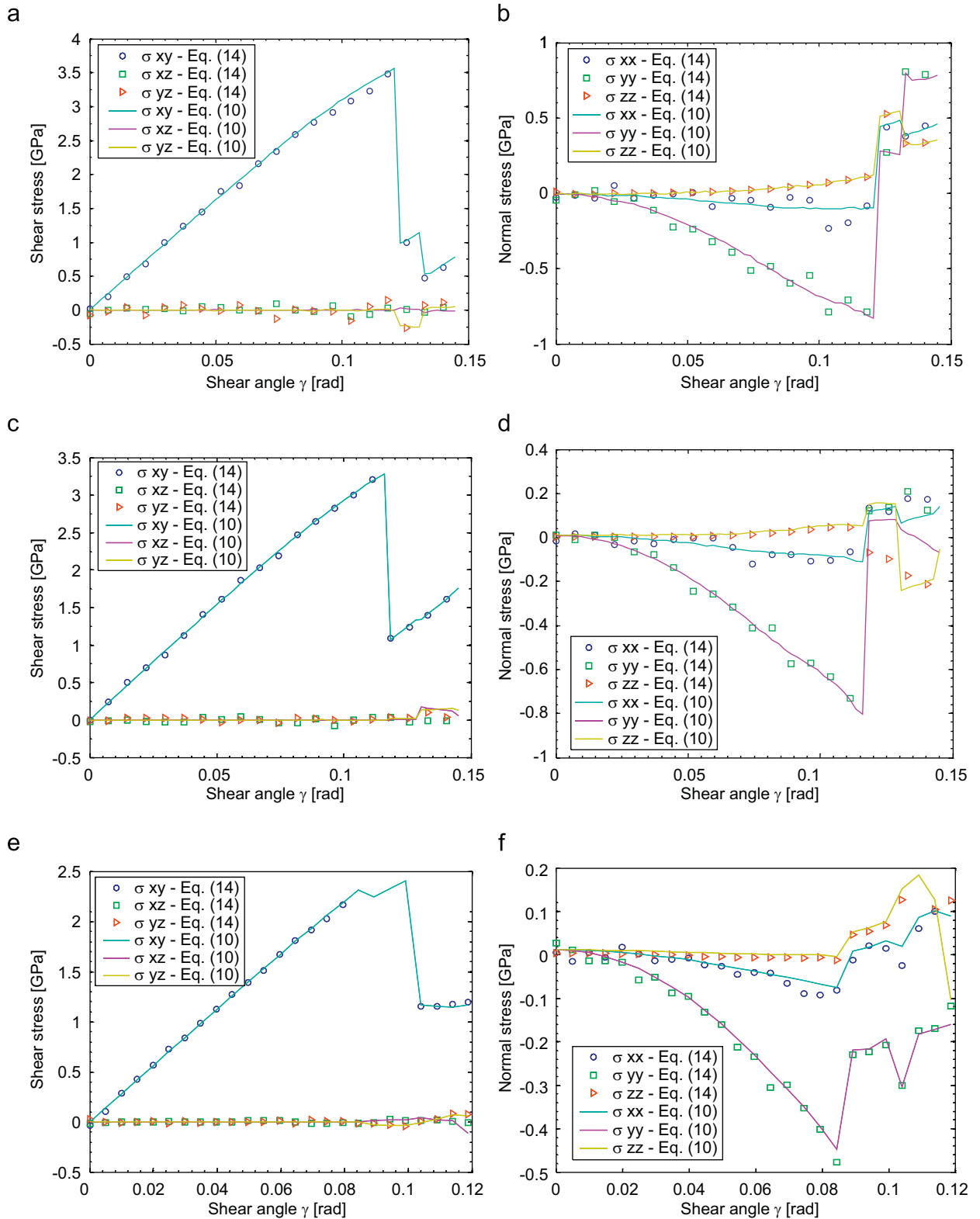


**Fig. 3.** Evolution with the shear angle  $\gamma$  of the averaged components of the Cauchy stress tensor for the shear test computed from Eqs. (10) and (14): (a), (c), (e)  $\sigma_{xy}$ ,  $\sigma_{xz}$ , and  $\sigma_{yz}$  for systems A, B, and C, respectively; (b), (d), (f)  $\sigma_{xx}$ ,  $\sigma_{yy}$ , and  $\sigma_{zz}$  for systems A, B, and C, respectively.

**Table 1**

From the results of the shear test, computed values of the shear modulus, the maximum shear stress, the shear stress at yield, the von Mises stress at yield, the maximum von Mises stress, the shear strain at the proportional limit, and the shear strain at yield

Specimen	$\gamma_{\text{linear}}$ (rad)	$\gamma_{\text{yield}}$ (rad)	$\sigma_{xy}^{\text{yield}}$ (GPa)	$\sigma_{xy}^{\text{max}}$ (GPa)	$\sigma_{\text{VM}}^{\text{yield}}$ (GPa)	$\sigma_{\text{VM}}^{\text{max}}$ (GPa)	$C_{44}$ (GPa)
A	0.044	0.121	3.562	3.562	6.230	6.230	32.229
B	0.037	0.116	3.285	3.285	5.750	5.740	31.077
C	0.035	0.084	2.315	2.408	4.030	4.180	28.264

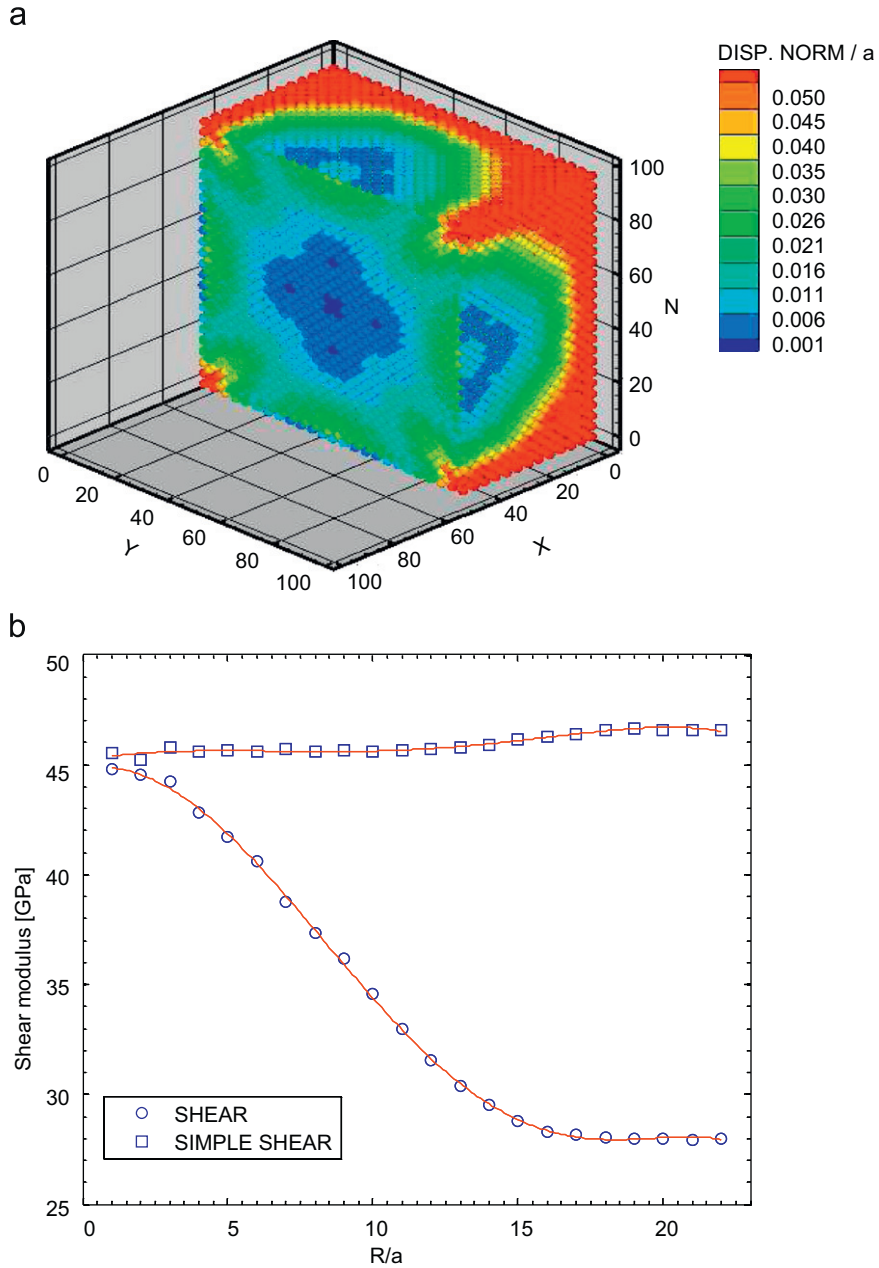


**Fig. 4.** (a) Reference configuration of system C; fringe plots give the magnitude of the normalized displacement vector in going from the perfect lattice configuration to the relaxed configuration (all distances in Å). (b) Variation of the shear modulus  $C_{44}$  with the radius of the sphere used to define the representative volume around the specimen centroid.

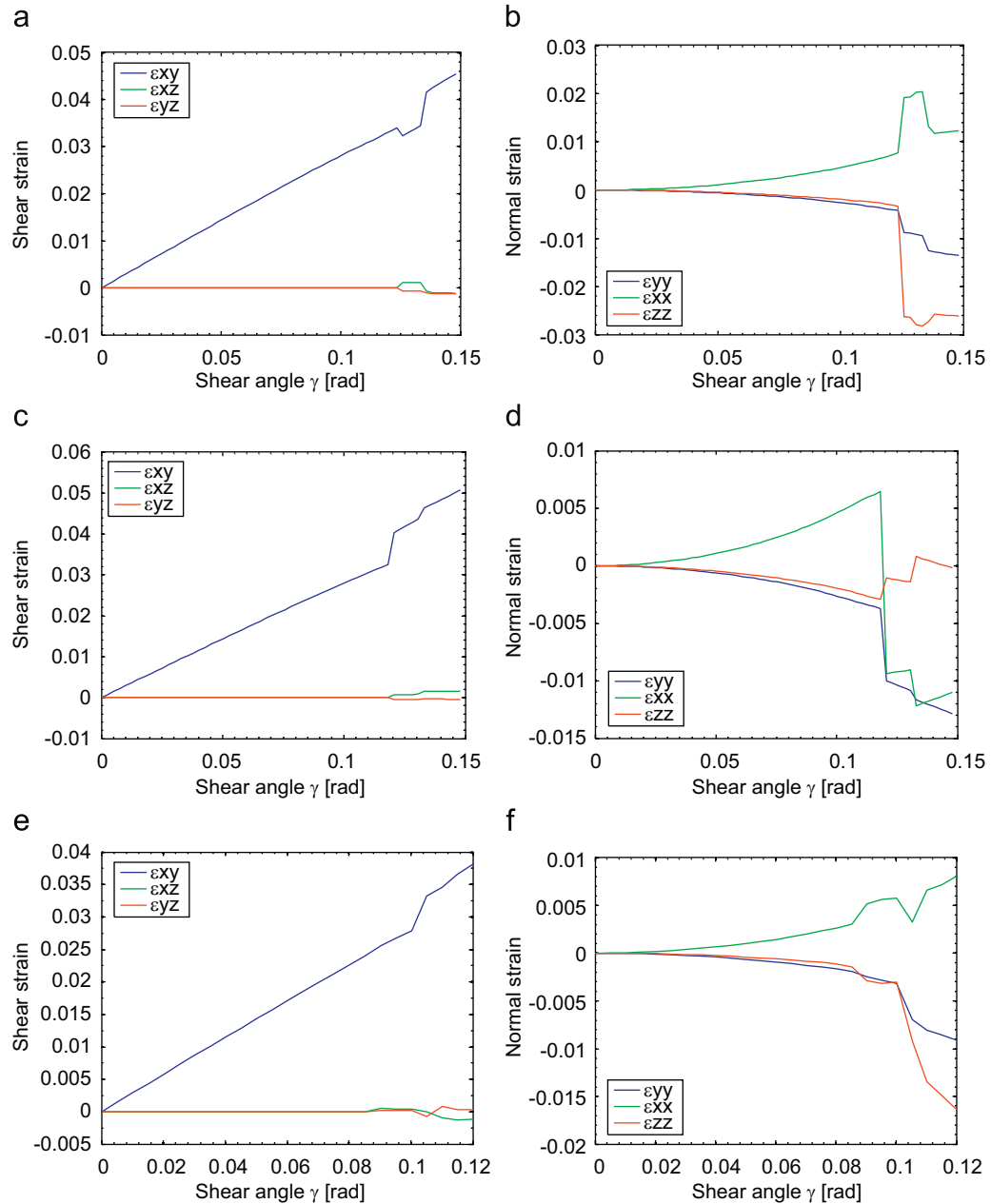


**Fig. 5.** Evolution with the shear angle  $\gamma$  of the averaged components of the Almansi–Hamel strain tensor for the shear test: (a), (c), (e)  $\epsilon_{xy}$ ,  $\epsilon_{xz}$ , and  $\epsilon_{yz}$  for systems A, B, and C, respectively; (b), (d), (f)  $\epsilon_{xx}$ ,  $\epsilon_{yy}$ , and  $\epsilon_{zz}$  for systems A, B, and C, respectively.

Ogata et al. (2004), using DFT, found relaxed and unrelaxed shear moduli of Au to equal 17.9 and 22.9 GPa, respectively. They applied an affine deformation to a perfect Au crystal to induce shear deformation along the  $\{1,1,1\}[-1,2,-1]$  slip system. Boundary conditions were adjusted so that the only two non-zero components of the strain and the stress tensors are those acting on the shear plane which is similar to that for pure torsional deformations of an isotropic linear elastic body. Clearly, the boundary-value problem studied here does not have ideal conditions simulated by Ogata et al. (2004). It can be seen from results exhibited in Fig. 3 that prior to the occurrence of sharp discontinuities in the stress–strain curves, the normal stress  $\sigma_{yy}$  has large negative values. The other two normal stresses,  $\sigma_{xx}$  and  $\sigma_{zz}$ , are negligible until the discontinuity appears in the stresses at  $\gamma = \gamma_{\text{yield}}$ . Thus the state of stress is quite different from that in Ogata et al.'s numerical simulation.

## 5.2. Simple shear test

Figs. 6 and 7 depict, respectively, evolutions with the shear angle  $\gamma$  of the average stresses and strains for the three specimens. In Table 2 we have summarized for the three specimens values of the shear stress, the von Mises stress, and  $\gamma$  at the proportionality limit and at the yield point. Magnitudes of all three compressive normal stresses increase with an increase in  $\gamma$  and are comparable to the magnitude of  $\sigma_{xy}$ . This is because all bounding planes are restricted from moving in normal directions. Thus in the absence of normal tractions applied to the bounding planes, the cube will expand. As for the shear test, the material exhibits the Poynting (1909) effect.

Fig. 6 also exhibits values of the average stress components computed from Eqs. (10), (14) and (21); the three sets of values agree with each other until  $\gamma = \gamma_{\text{yield}}$ . At  $\gamma = \gamma_{\text{yield}}$  stress components computed for the equivalent hyperelastic body do not show any sudden drop, and the slope of the  $\sigma_{xy}$  vs.  $\gamma$  curve continues to increase. One may say that the hyperelastic body exhibits a hardening effect in the sense that its tangent modulus continues to increase with an increase in  $\gamma$ . The close agreement between stresses computed from results of MM simulations and the analytic expression verifies our code, and validates the MM results. Evolutions of strains plotted in Fig. 7 reveal that Eqs. (8) and (16.2) give nearly the same values of strain components.

The value of  $\sigma_{xy}^{\text{yield}}$  derived from the results of the simple shear deformations is nearly four times that from the shear test results. Even for system C with 58,825 atoms, the two values of the yield stress differ noticeably. The main difference between the tests is the presence of four free surfaces in the shear deformations and no free surface in the simple shear deformations. For the simple shear test involving displacements prescribed on all bounding surfaces, the onset of local instabilities is delayed, that increases the yield stress.

The slope of the average shear stress  $\sigma_{xy}$  vs. the shear angle  $\gamma$  for  $\gamma \leq \gamma_{\text{linear}}$  gives values for the shear modulus  $C_{44}$  equal to 51.64, 49.88, and 46.40 GPa for specimens A, B, and C, respectively. These values are closer to the 45 GPa than those derived from simulations of the shear test, and converge to this value with an increase in the number of atoms in the system. As shown in Fig. 4b, the computed value of  $C_{44}$  for SRVs of different radii centered at specimen's centroid is nearly constant and equals 45.5 GPa.

## 5.3. Comparison between different measures of the average Cauchy stress tensor

In Fig. 8 we have plotted the evolution of the average shear stress  $\sigma_{xy}$  for system B computed with the following four definitions: the configurational part of the virial stress tensor (Eq. (10)), the total force acting on atoms at the bounding surfaces (Eq. (14)), the average local stress tensor (Eq. (15)), and the Mechanics of Materials approach (the tangential force per unit surface area). It is evident that all these stresses agree with each other. During the computation of average stresses from the virial and the local stress tensors, all atoms in the system, including those with prescribed displacements, were considered. In the limit of very large number of atoms in the system, using only active or all atoms in the computation of stresses should give essentially the same results. We note that the average shear stress computed from the total tangential force acting on the top and the bottom surfaces agrees well with that obtained by using Eqs. (10), (14) and (15).

For both shear and simple shear tests, values of the shear modulus and the yield stress determined with different ways of finding average stresses are summarized in Table 3. It is clear that these methods give nearly the same values of the shear modulus and the yield stress. However, their values for the shear and the simple shear tests are different.

## 6. Analysis of instabilities

### 6.1. Instability criteria

#### 6.1.1. Local instability

We assume that an atom is stable at the position  $\mathbf{r}^{(i)}$  if its potential energy  $V^{(i)}$  there is minimum. Recall that while finding the relaxed configuration of a system of atoms, the sum of potential energies of all atoms, but not every atom, is minimized. Thus it is possible that the overall system is in stable equilibrium, but one or more atoms are either in neutral or unstable equilibrium positions.

An alternative criterion for local stability is the following. An atom in its present position is stable provided that an acceleration wave can propagate through that point. Since the wave speed is proportional to an eigenvalue of the acoustic tensor, one can ascertain the local stability of an atom by finding eigenvalues of the acoustic tensor evaluated in the deformed configuration of the atomic system.

Following Hill (1962), van Vliet et al. (2003) postulated a criterion for the stability of a representative volume composed of a discrete number of particles and termed it the  $\mathcal{A}$  criterion. That is, a material point is unstable if

$$\mathcal{A}(\mathbf{w}, \mathbf{n}) = (C_{\alpha\beta\phi\rho} w_\alpha w_\phi + \sigma_{\beta\rho}) n_\beta n_\rho \leq 0, \quad (22)$$

where  $C_{\alpha\beta\phi\rho}$  are components of the isothermal elasticity tensor,  $\mathbf{w}$  is the polarization vector and  $\mathbf{n}$  is the wave vector. The authors postulated that a local instability initiates at the spatial position where the minimum value of  $\mathcal{A}$  vanishes.

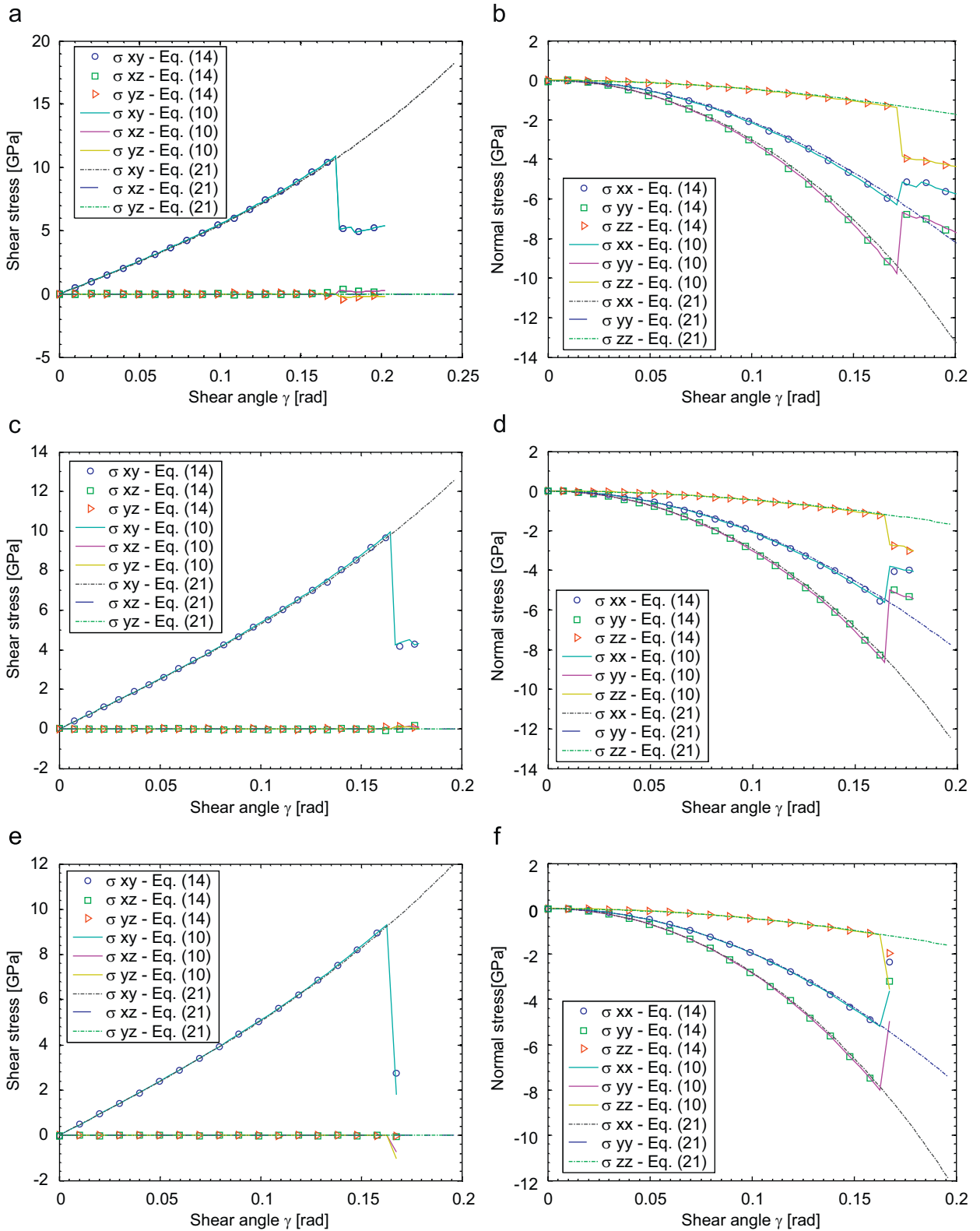


**Fig. 6.** Evolution with the shear angle  $\gamma$  of the averaged components of the Cauchy stress tensor for the simple shear test computed from Eqs. (10), (14), and (21): (a), (c), and (e)  $\sigma_{xy}$ ,  $\sigma_{xz}$ , and  $\sigma_{yz}$  for systems A, B, and C, respectively; (b), (d), and (f)  $\sigma_{xx}$ ,  $\sigma_{yy}$ , and  $\sigma_{zz}$  for systems A, B, and C, respectively.

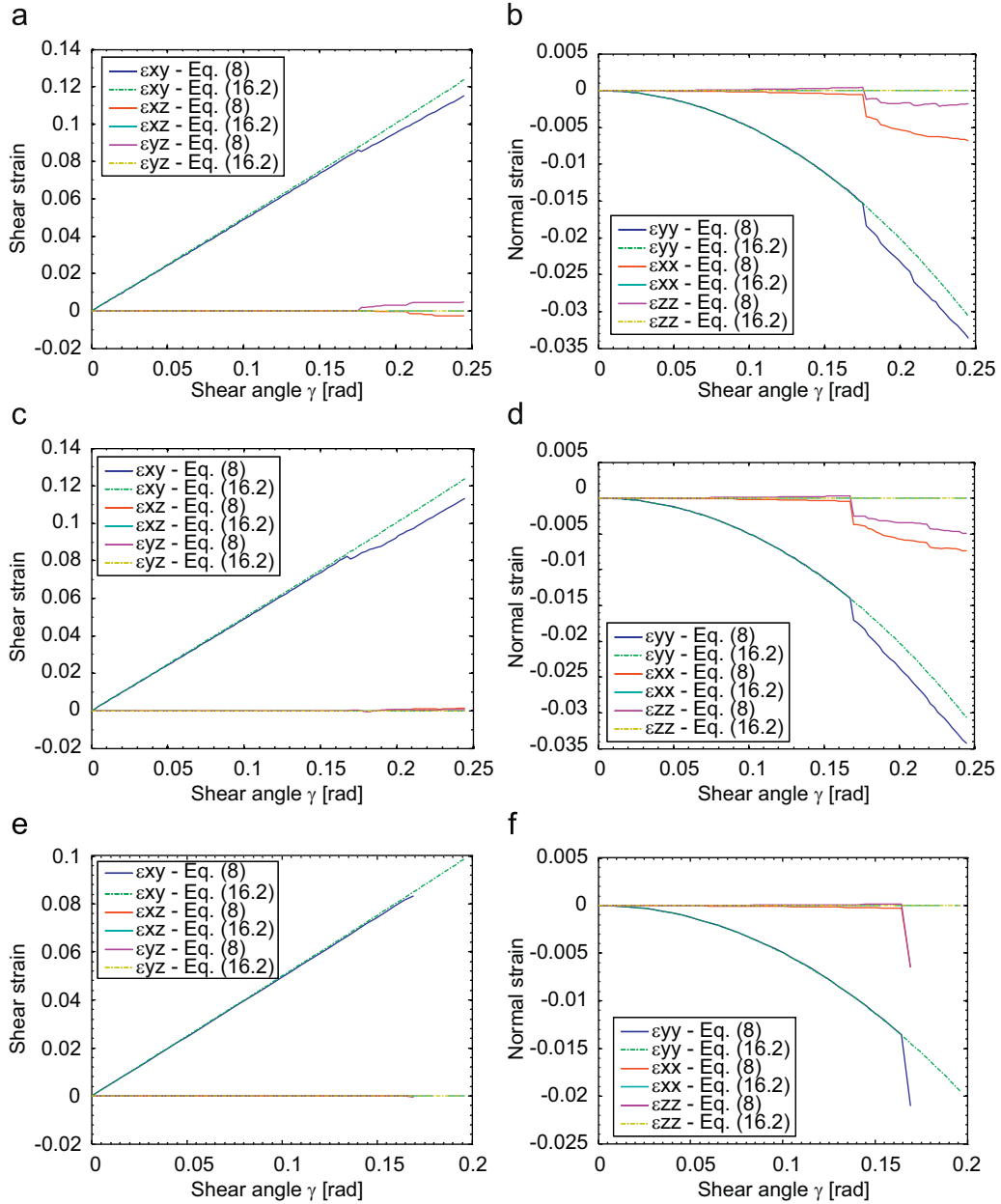


**Fig. 7.** Evolution with the shear angle  $\gamma$  of the average values of components of the Almansi–Hamel strain tensor for the simple shear test computed with the MSPH method and Eqs. (8) and (16.2); (a), (c), and (e)  $\epsilon_{xy}$ ,  $\epsilon_{xz}$ , and  $\epsilon_{yz}$  for systems A, B, and C, respectively; (b), (d), and (f)  $\epsilon_{xx}$ ,  $\epsilon_{yy}$ , and  $\epsilon_{zz}$  for systems A, B, and C, respectively.

**Table 2**

From the results of the simple shear test, computed values of the shear modulus, the maximum shear stress, the shear stress at yield, the von Mises stress at yield, the maximum von Mises stress, the shear strain at the proportional limit, and the shear strain at yield

Specimen	$\gamma_{\text{linear}}$ (rad)	$\gamma_{\text{yield}}$ (rad)	$\sigma_{xy}^{\text{yield}}$ (GPa)	$\sigma_{xy}^{\text{max}}$ (GPa)	$\sigma_{VM}^{\text{yield}}$ (GPa)	$\sigma_{VM}^{\text{max}}$ (GPa)	$C_{44}$ (GPa)
A	0.050	0.173	10.780	10.780	20.220	20.220	51.644
B	0.043	0.165	9.944	9.944	18.390	18.390	49.883
C	0.040	0.162	9.170	9.170	17.190	17.190	46.401

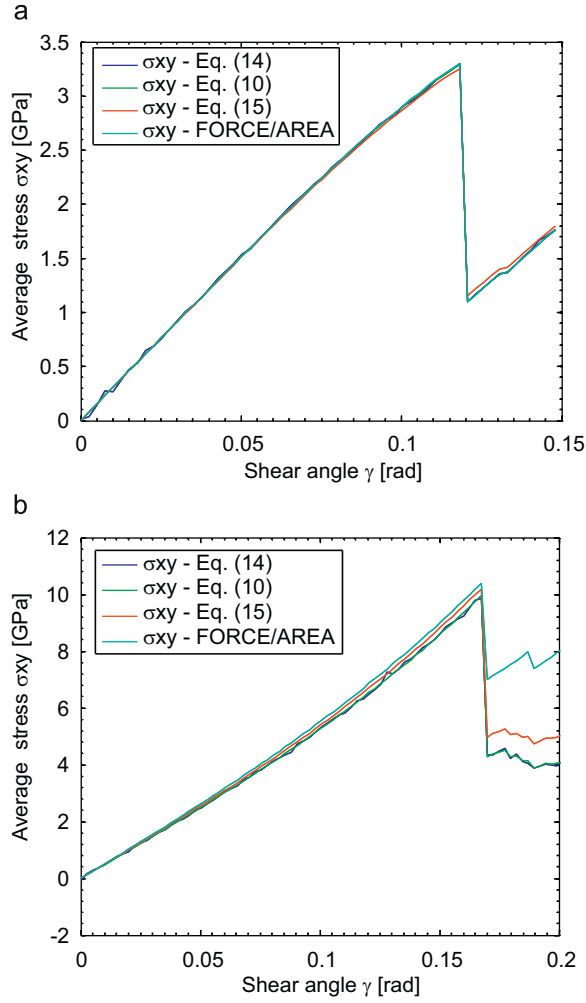


**Fig. 8.** Comparison between different stress measures of the averaged Cauchy stress tensor for system B in the shear and the simple shear test, Eqs. (10), (14), (15) and the Mechanics of Materials approach (force/area): (a) shear test and (b) simple shear test.

**Table 3**

Comparison of the shear modulus and the yield stress computed with different averaged stresses for system B

Method	Shear		Simple shear	
	Shear modulus $C_{44}$ (GPa)	Yield stress $\sigma_{xy}^{\text{yield}}$ (GPa)	Shear modulus $C_{44}$ (GPa)	Yield stress $\sigma_{xy}^{\text{yield}}$ (GPa)
Eq. (14)	31.375	3.304	52.802	9.857
Eq. (10)	31.077	3.285	49.883	9.944
Eq. (15)	30.346	3.254	49.904	10.187
Force/area	30.399	3.304	51.272	10.383

Lu and Zhang (2006) have proposed that the atomic acoustic tensor  $\mathbf{Q}^{(i)}$  defined by

$$Q_{\alpha\beta}^{(i)}(\hat{\mathbf{n}}) = \sum_{\substack{j=1 \\ j \neq i}}^{Ne} \sum_{\substack{k=1 \\ k \neq i}}^{Ne} (\mathbf{r}^{(ij)} \cdot \hat{\mathbf{n}}) \frac{\partial V^{(i)}}{\partial r_{\alpha}^{(ij)} \partial r_{\beta}^{(kl)}} (\mathbf{r}^{(kl)} \cdot \hat{\mathbf{n}}) \quad (23)$$

be used instead of the  $A$  criterion to characterize local instabilities; in Eq. (23),  $|\hat{\mathbf{n}}| = 1$ . Thus an atom is stable in the present position if and only if all eigenvalues of  $\mathbf{Q}^{(i)}$  there are positive. Equivalently, the position of an atom is unstable if  $\det[\mathbf{Q}^{(i)}] = 0$ .

The condition that all eigenvalues of the local acoustic tensor  $\mathbf{Q}^{(i)}$  be positive is equivalent to requiring that the potential energy of atom  $i$  given by Eq. (1) be a convex function of the relative position vectors between atom  $i$  and all other atoms.

For simulations of the shear and the simple shear deformations described above, we compute  $\mathbf{Q}^{(i)}$  after every increment in the prescribed displacements, and find the unit vector  $\hat{n}$  that minimizes eigenvalues of  $\mathbf{Q}^{(i)}$ . If the lowest eigenvalue of  $\mathbf{Q}^{(i)}$  is non-positive, then the atom is unstable in the present position. Note that the unit vector  $\hat{n}$  can be expressed in terms of the longitude and the latitude angles as  $\hat{n} = [\cos \varphi \cos \theta, \cos \varphi \sin \theta, \sin \varphi]$ . Thus we need to find angles  $\phi$  and  $\theta$  in the range  $0 \leq \theta \leq 2\pi$  and  $-\pi/2 \leq \varphi \leq \pi/2$  that minimize eigenvalues of  $\mathbf{Q}^{(i)}$ . We accomplish this by evaluating the determinant of  $\mathbf{Q}^{(i)}$  on a grid of 1800 points obtained by dividing the ranges for  $\phi$  and  $\theta$  into equal segments of length  $\pi/30$ .

Steinmann et al. (2007) have used molecular dynamics simulations to study simple shear and uniaxial tensile deformations of an FCC crystal oriented in the {1,1,1} plane. They related the local (material) instability with the loss of ellipticity expressed by the Legendre–Hadamard condition (Truesdell and Noll, 1992). That is, the acoustic tensor  $\mathbf{Q}$  at a material point of a continuous system given by

$$Q(\hat{N})_{ik} = L_{iMkK} \hat{N}_M \hat{N}_K \tag{24}$$

is singular for a unit vector  $\hat{N}$ . In Eq. (24)

$$L_{iMkK} = \frac{\partial \bar{P}_{iM}}{\partial F_{kK}} \tag{25}$$

is the elasticity matrix evaluated at the present value of  $\mathbf{F}$ , and the unit vector  $\hat{N}$  gives the direction of propagation of the disturbance in the reference configuration. An eigenvector of  $\mathbf{Q}$  is parallel to the disturbance vector. Steinmann et al. (2007)

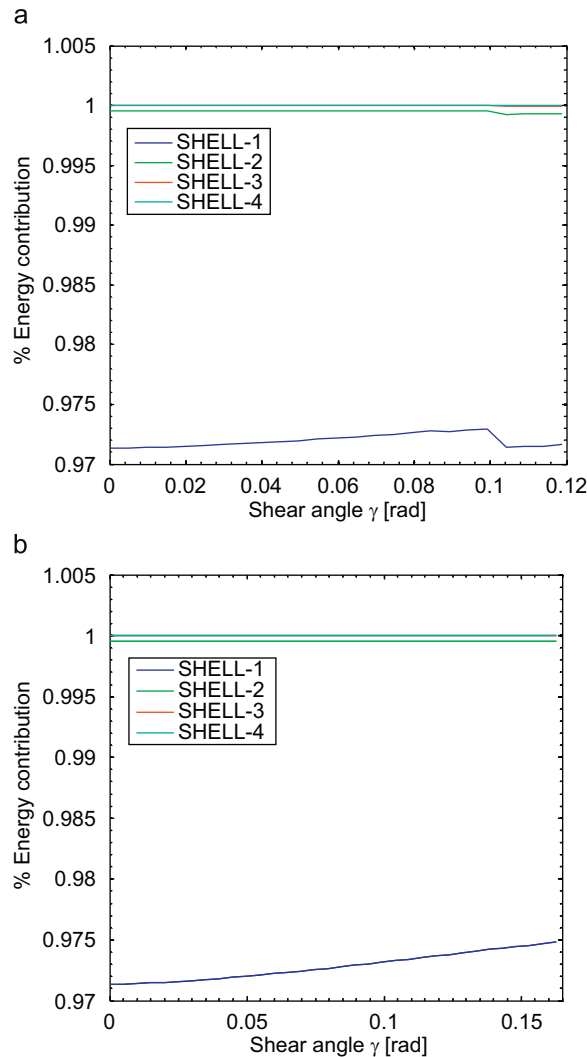


**Fig. 9.** Variation of the local energy due to contributions of different number of neighboring atoms. These values are obtained from energies at the centroid of system C. The blue line is the percentage of the total energy due only to atoms in shell 1; other curves are for atoms in shells 2, 3, and 4: (a) shear test and (b) simple shear test.

found that the strain at which the determinant of  $\mathbf{Q}$  vanished coincided with that at which deformations departed from those dictated by the prescribed boundary conditions. The effect of boundaries was suppressed by prescribing displacements of atoms near the bounding surfaces so that other atoms in the interior did not interact with under-coordinated atoms (the coordination number is the total number of nearest neighbors of a central atom, and equals 12 for an FCC crystal). For the Au crystal this can be generally satisfied by prescribing displacements of atoms within 6 Å of the bounding planes.

Recently Miller and Rodney (2008) performed 2D and 3D simulations of nano-indentation of an FCC crystal. Based on the results of their simulations, they proposed that the initiation of an instability at an atomic position is not due to deformations in the neighborhood of that point but is the result of deformations at several atoms surrounding the one whose stability is being studied. Furthermore, they showed that a vanishing of the eigenvalue of the Hessian matrix corresponding to the d.o.f. of atoms within the surrounding region implied the nucleation of a local instability.

In an attempt to correlate the onset of local instabilities with highly inhomogeneous deformations near the specimen boundaries, we propose that an atom  $i$  becomes unstable when the energy  $V^{(i)}$  due to atoms in the SRV with  $R = (\sqrt{3}/2)a \text{ \AA}$  ceases to be positive definite; atoms in the SRV of  $R = (\sqrt{3}/2)a \text{ \AA}$  are usually referred to as those within the first shell of atom  $i$ . For a pristine FCC crystal, the number of atoms in the first shell of an atom equals 12. This criterion is motivated by the form of the inter-atomic TB potential and the observation that the contribution to the local energy from these atoms is more than 97% of that due to all atoms in the system, and this is so even when an atom is close to a free surface; e.g., see Fig. 9 in which the energy of atom  $i$  due to contributions from atoms in shells 1, 2, 3, and 4 are plotted. Shells 2, 3, and 4 are SRVs with  $R$  approximately equal to  $(3/2)(\sqrt{3}/2)a$ ,  $\sqrt{3}a$ , and  $(5/2)(\sqrt{3}/2)a \text{ \AA}$ , respectively. Thus an atom becomes unstable when the local Hessian matrix

$$H_{jk}^{(i)} = \sum_{\substack{k=1 \\ k \neq i}}^{N_f} \sum_{\substack{j=1 \\ j \neq i}}^{N_f} \frac{\partial^2 V^{(i)}}{\partial r^{(ij)} \partial r^{(ik)}} \quad (26)$$

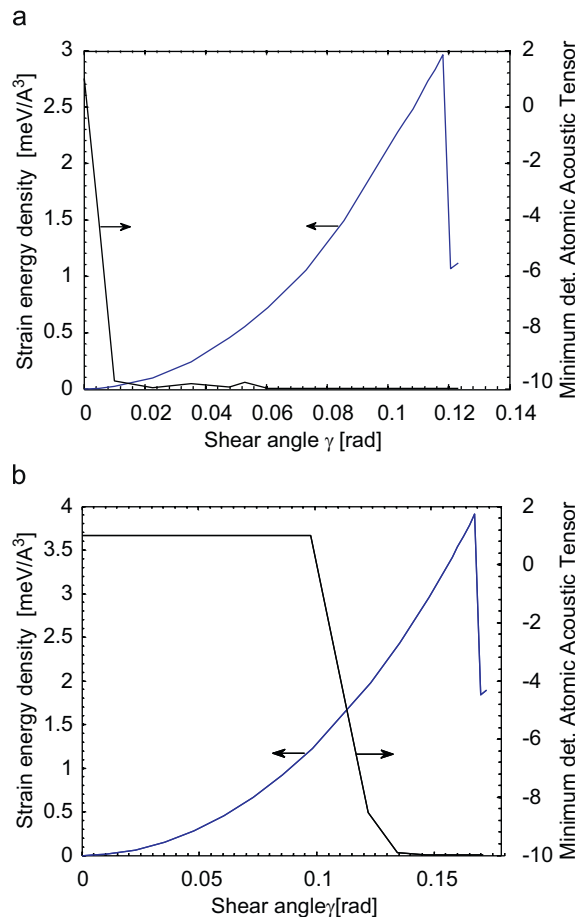


**Fig. 10.** Variations with the shear angle  $\gamma$  of the total strain energy density (blue line) and the minimum value of the determinant of the atomic acoustic tensor  $\mathbf{Q}^{(i)}$  for system B: (a) shear test and (b) simple shear test.

has a non-positive eigenvalue. Here  $N_f$  equals the number of atoms in the first shell of atom  $i$ . The condition for local stability is therefore  $\min\{\lambda_k^{(i)}\} > 0$ , where  $\lambda_k^{(i)}$  is an eigenvalue of  $\mathbf{H}^{(i)}$ .

In order to find a correlation, if any, between atoms that become locally unstable and also have a relatively large value of the CNP we compute the CNP for atom  $i$  defined by

$$\text{CNP}^{(i)} = \frac{1}{N_f} \sum_{j=1}^{N_f} \left| \sum_{k=1}^{N_{ij}} (\mathbf{r}^{(ik)} + \mathbf{r}^{(jk)}) \right|^2, \quad (27)$$

where  $N_{ij}$  is the number of common neighbors between atoms  $i$  and  $j$ . For a perfect crystal the value of the CNP for every interior atom is essentially zero; it exceeds 20 for atoms on bounding surfaces, and is greater than 2 for atoms located at points where crystallographic defects appear.

Finally we explore a correlation between regions of local instabilities and those of relatively large values of one or more components of  $\mathbf{G}$ .

### 6.1.2. Global instability

As in continuum mechanics, the configuration of a system comprised of a collection of atoms is globally stable if the potential energy of the system in that configuration is minimum. The potential energy equals the strain energy of deformation less the work done by external forces. For boundary conditions considered here (i.e., either displacements or null external force prescribed), the potential energy of the system equals its strain energy which for the discrete system being studied equals the sum of strain energies of all atoms in it.

For potential energy of the system to be minimum, the Hessian matrix with elements equaling second derivatives of the potential energy with respect to relative position vectors between atoms in the current configuration and evaluated at their current positions must be positive definite. Equivalently, all eigenvalues of this Hessian matrix must be positive. When computing eigenvalues of the Hessian matrix, rows and columns corresponding to atoms with prescribed displacements are eliminated to get the reduced Hessian matrix. With each atom having three d.o.f., the size of the reduced Hessian matrix equals  $3N_a \times 3N_a$  where  $N_a$  equals the number of active atoms in the system being studied. Thus the system of atoms will become globally unstable when at least one eigenvalue of the reduced Hessian matrix equals zero.

In terms of the *Considerè criterion* (1888), the system will become globally unstable when the load (which for the shear and the simple shear deformations implies the shear stress in the plane of deformation) becomes the maximum. Thus at the onset of the global instability, the shear stress–shear angle curve will exhibit a sharp discontinuity.

## 6.2. Results of numerical simulations

### 6.2.1. Local instabilities

**6.2.1.1. Shear test.** The local instability criterion in terms of the minimum eigenvalue of the local acoustic tensor  $\mathbf{Q}^{(i)}$  becoming non-positive predicted instabilities for small values of the shear angle when no discontinuity in a stress–strain curve or a change in the curvature of the local energy vs. the shear angle curve was observed. Fig. 10a shows variation with the shear angle of the minimum value of the determinant of  $\mathbf{Q}^{(i)}$  for any atom in system B. Atoms where instabilities first occurred are located close to the left and the right free surfaces of the system.

We note that the strain energy density vs. the shear angle curve in Fig. 10a exhibits a discontinuity at the value of the shear angle that is much larger than the one where  $\det[\mathbf{Q}^{(i)}] = 0$ .

Fig. 11a exhibits the evolution of the minimum eigenvalue of the local Hessian  $\mathbf{H}^{(i)}$  among all atoms in the system where displacements are not prescribed. This value remains positive until  $\gamma = 0.066$ , 0.053, and 0.042, respectively, for systems A, B, and C, when the minimum eigenvalue of  $\mathbf{H}^{(i)}$  becomes negative and stays negative during subsequent deformations for at least one atom in the specimen. Fig. 11b shows evolution of the fraction of atoms that have become unstable. This percentage increases rapidly for system C. The increase in the number of unstable atoms is very similar for specimens A and B. The dashed vertical lines correspond to the shear angle values at which the global instability ensues (see Section 6.2.2). It is clear that for each one of the three specimens only about 8% of atoms have become unstable just prior to the onset of the global instability, and this number has increased to nearly 30% for systems B and C, and ~50% for system A at the end of the drop in the total energy density vs. the shear angle curve.

Fig. 12 shows, for system C, distributions of the minimum eigenvalue of  $\mathbf{H}^{(i)}$  and the CNP. Figs. 12a and b correspond to the strain level when local instabilities were detected first at  $\gamma = 0.042$ . Only atomic positions where the local instability condition has been satisfied are depicted in Figs. 12a, c, e, g, and t. Similarly, only atoms with high values of the CNP are exhibited in Figs. 12b, d, f, h, and u. The eight blue points in Fig. 12a are diametrically opposite to each other and are in regions where the atomic volume  $\Omega^{(i)}$  is greater than its value in the reference configuration; i.e.,  $\det(\mathbf{F}^{(i)}) > 1$ . In Fig. 12b only atoms at the bounding surfaces have large values of the CNP.

Figs. 12c and d correspond to the shear angle of 0.0872 that is just prior to the occurrence of the first discontinuity in the  $\sigma_{xy}-\gamma$  curve; at this point the number of unstable atoms has increased mainly in the four corners and in the top and the bottom surfaces (planes parallel to the  $xz$  plane). It can be observed that unstable atoms are distributed in 10 sub-volumes symmetrically distributed with respect to planes passing through the diagonals of the  $xy$  plane. If one excludes atoms on the bounding surfaces, then there is a reasonable correlation between atoms having large values of the CNP and those

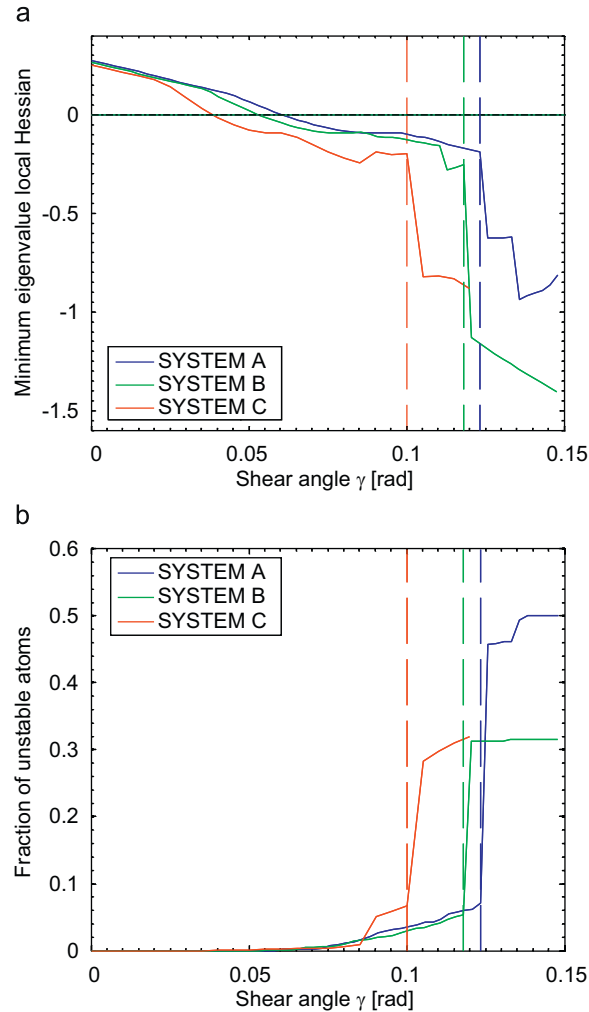


**Fig. 11.** For the shear test, variation with the shear angle  $\gamma$  of (a) the minimum eigenvalue of the Hessian of the local energy and (b) the fraction of unstable atoms.

where the minimum eigenvalue of the local Hessian matrix is non-positive. Figs. 12e and f correspond to the shear angle of 0.0921 that is just after the first steep drop in the  $\sigma_{xy}$ - $\gamma$  curve; it can be observed that on the edges  $Y = Y_{\max}$ ,  $X = 0$  and  $Y = 0$ ,  $X = X_{\max}$  groups of new unstable atoms have appeared. These new atoms are located on crystallographic planes  $\{1,1,1\}$  of high density where shear deformation is accommodated by changing the stacking sequence in the crystal. As for the previous case, these atomic positions correlate well with the interior atoms exhibited in Fig. 12f where the CNP has relatively high values. Figs. 12g and h correspond to the shear angle of 0.102 just prior to the system becoming globally unstable when the most pronounced drop in the  $\sigma_{xy}$ - $\gamma$  curve occurs. Between the instants of  $\gamma = 0.0921$  and 0.102, considerably more atoms have become unstable. Figs. 12t and u correspond to the shear angle of 0.1069 that corresponds to the strain level right after the sharp drop in the  $\sigma_{xy}$ - $\gamma$  curve when nearly 30% of atoms in the system have become unstable. Atoms with non-positive values of the minimum eigenvalue of the local Hessian matrix  $\mathbf{H}^{(i)}$  and those with large values of the CNP are similarly situated, and their numbers are essentially equal. We have not investigated if a large value of the CNP corresponds to a higher magnitude of the negative eigenvalue of  $\mathbf{H}^{(i)}$ . However, results presented in Fig. 12 imply that there is a good correlation between locations of unstable atoms and those having a large value of the CNP.

For system C, Fig. 13 exhibits atoms with a large value of the norm  $\|G\|$  defined by

$$\|G\| = (a \max(|G_{\alpha\beta\gamma}|)).$$

Here  $\max(|G_{\alpha\beta\gamma}|)$  equals the maximum value of any one of the 27 components of  $\mathbf{G}$  at any point in the system, and it is multiplied by the lattice parameter  $a$  to get a non-dimensional number. Results plotted in Figs. 13a and b correspond to  $\gamma = 0.0872$  and 0.0921, respectively; that is, instants immediately preceding and following the first drop in the shear stress-shear angle curves. Results plotted in Figs. 12c–f also correspond to these strain levels. Figs. 13c and d correspond to

$\gamma = 0.102$  and  $0.1069$ , respectively, the same values of the shear angle for which results are depicted in Figs. 12g,h and t,u. We note that regions with a large value of  $\|G\|$  have high inhomogeneous deformations.

Atoms evinced in Figs. 13c and d having a large value of  $\|G\|$  when compared with those included in Figs. 12g,h and t,u suggest that shapes and locations of geometric regions of high values of  $\|G\|$ , large values of the CNP, and non-positive values of the minimum eigenvalue of  $\mathbf{H}^{(i)}$  are essentially identical. Thus any one of these three criteria can be used to characterize a local instability. Each one of these three methods predicts that atoms on a bounding plane become unstable

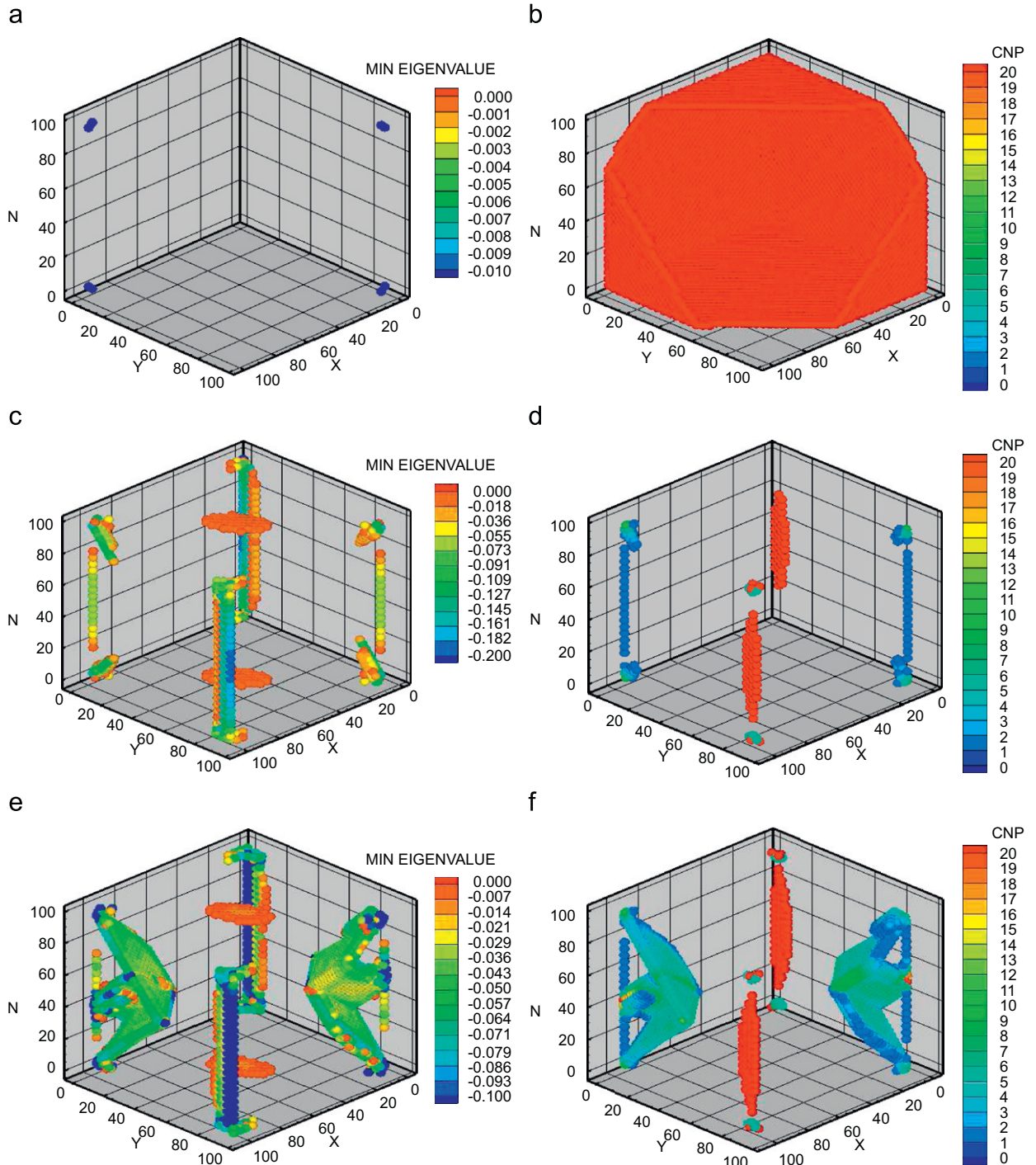


**Fig. 12.** Distribution of the minimum eigenvalue of the local Hessian, and the CNP for the shear test in system C: (a, b)  $\gamma = 0.0426$ , (c, d)  $\gamma = 0.0872$ , (e, f)  $\gamma = 0.0921$ , (g, h)  $\gamma = 0.102$ , and (t, u)  $\gamma = 0.1069$ .

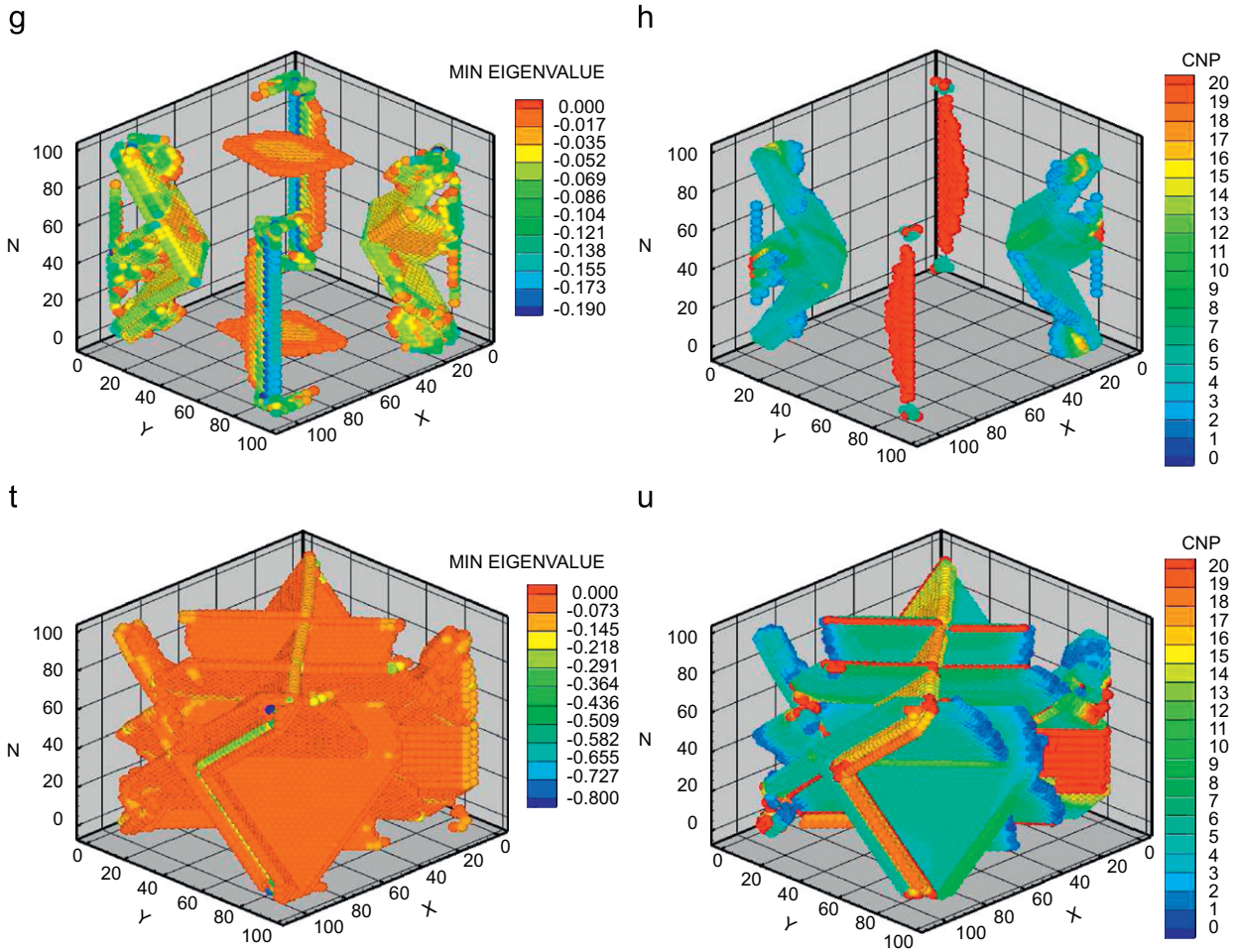


Fig. 12. (Continued)

first. However, the local instability does not seem to propagate from atoms on the boundaries to those in the interior of the cube since the interior unstable atoms are not necessarily bonded to those on the bounding surfaces.

Fig. 14 shows the variation of the derivative with respect to  $\gamma$  of the expected value  $\langle \|G\| \rangle$  of  $\|G\|$  computed from a kernel approximation of the probability density function of its distribution at each load step. From the probability density functions (not shown) for  $\gamma = 0.0227$  and  $0.0426$ , the distributions of  $\|G\|$  in the specimen are essentially zero and the expected values are  $0.0104$  and  $0.0138$ , respectively. Between these two configurations the change in the expected value with respect to  $\gamma$ ,  $d\langle \|G\| \rangle/d\gamma$ , is only  $0.171$ . From the probability densities for  $\gamma = 0.0872$  and  $0.0921$  which correspond to distributions shown in Figs. 12c and f,  $d\langle \|G\| \rangle/d\gamma = 0.755$  which is substantially higher than  $0.171$ . Similarly, between  $\gamma = 0.102$  and  $0.1069$ ,  $d\langle \|G\| \rangle/d\gamma = 6.26$ . Thus a large value of  $d\langle \|G\| \rangle/d\gamma$  also signifies that a major part of the system has undergone severe inhomogeneous deformations, and has become locally unstable.

**6.2.1.2. Simple shear test.** For the simple shear test, non-positive values of the minimum eigenvalue of  $\mathbf{Q}^{(i)}$  were found at atoms close to the bounding surfaces just prior to the system becoming globally unstable. None of the local instability criteria are satisfied for values of the shear angle  $\gamma$  that are noticeably less than the one where the system becomes globally unstable.

Fig. 15a exhibits the evolution of the minimum eigenvalue of the local Hessian  $\mathbf{H}^{(i)}$ . Unlike in the shear test, no pronounced local inhomogeneities occur before the onset of the global instability. It could be due to the fact that displacements prescribed on all bounding surfaces constrain deformations of all interior atoms. The first local instability at four atoms occurs simultaneously just prior to the onset of the global instability at  $\gamma = 0.155$ , and the relative positions of the four atoms and the shear strain at the onset of the instability are essentially independent of the specimen size. Nearly 40% of atoms become unstable at  $\gamma = 0.1752$ ,  $0.1675$ , and  $0.1644$  for specimens A, B, and C, respectively. Fig. 15a also shows the evolution of the minimum eigenvalue of the local Hessian for the hyperelastic material. Although the minimum eigenvalue of the Hessian decreases with an increase in the shear strain, it does not become negative. Since the shear stress

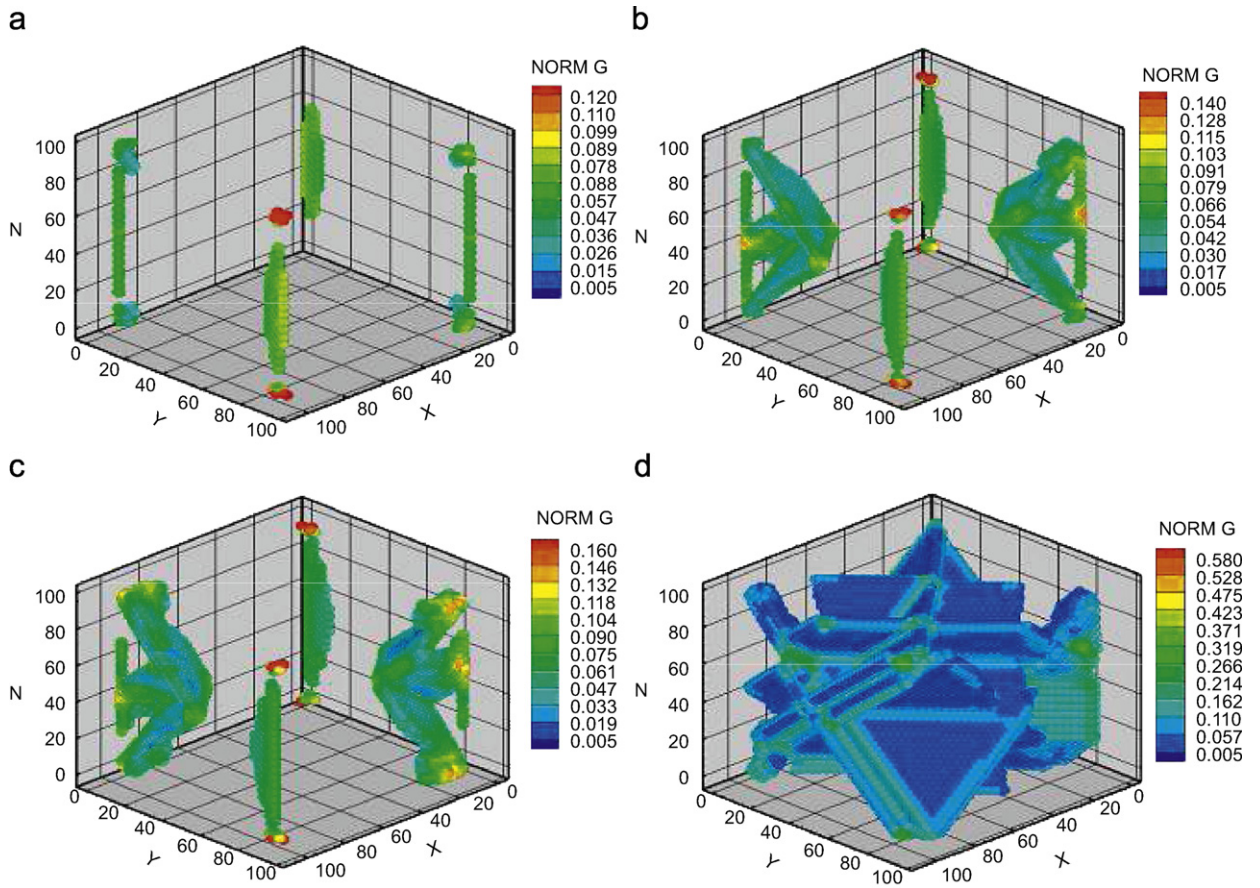


Fig. 13. Distribution of the norm ( $a \max(|G_{x\beta\gamma}|)$ ) of  $G$  for the shear test in system C: (a)  $\gamma = 0.0872$ , (b)  $\gamma = 0.0921$ , (c)  $\gamma = 0.102$ , and (d)  $\gamma = 0.1069$ .

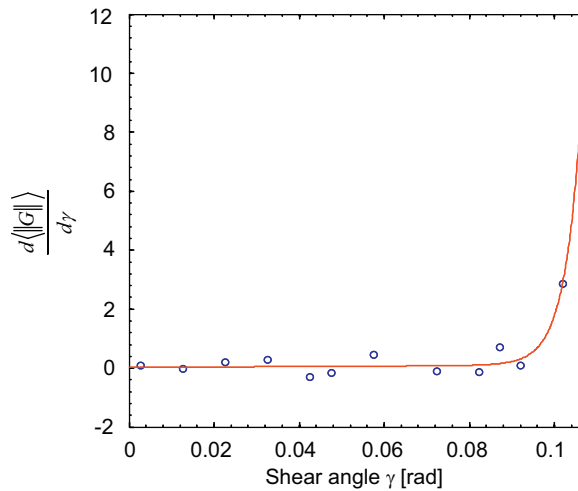
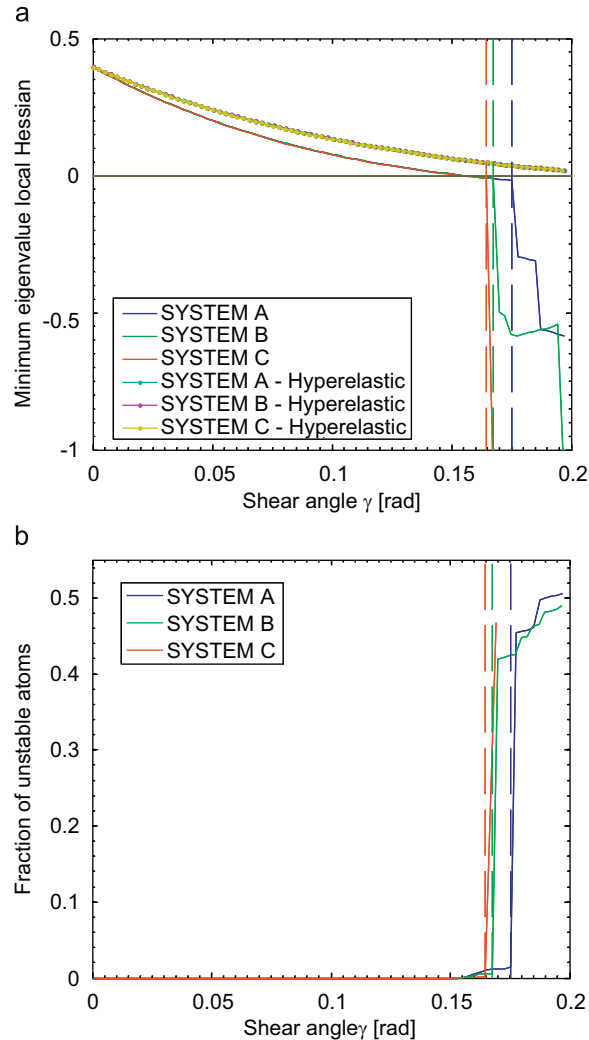


Fig. 14. Derivative with respect to  $\gamma$  of the expected value of the norm ( $a \max(|G_{x\beta\gamma}|)$ ) of  $G$  for shear test in system C.

vs. the shear strain curve for the hyperelastic material basically coincides with that derived from the MM simulations till the onset of instabilities, it is reasonable to conclude that the Cauchy–Born rule used to derive the strain energy density from the atomic potential holds for averaged quantities till the initiation of instabilities.



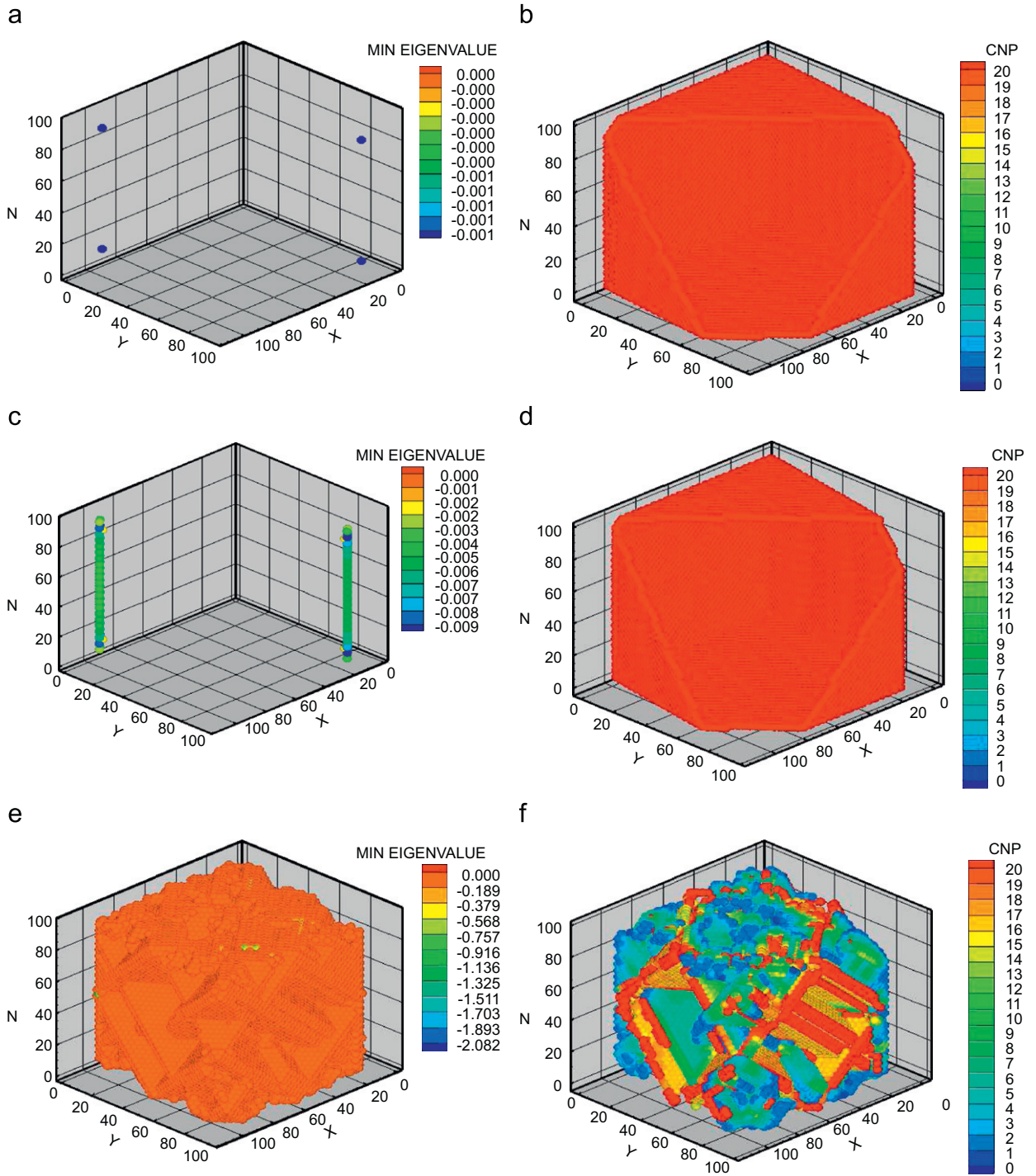
**Fig. 15.** For the shear test, variation with the deformation of (a) the minimum eigenvalue of the Hessian of the local energy, and (b) the percentage of unstable atoms.

Fig. 16a shows locations of the four atoms where local instabilities ensue for system C at  $\gamma = 0.155$ . In Figs. 16a, c and e positions of only unstable atoms are exhibited. At  $\gamma = 0.1655$  two geometrically opposite columns of unstable atoms have formed (see Fig. 16c). After the next load step,  $\gamma = 0.1703$ , a considerable number of atoms distributed over atomic planes in the interior of the system have become unstable. Thus both local and global instabilities occur almost simultaneously in the simple shear test but the initiation of local instabilities precedes that of the global instability by a large value of the shear strain in the shear test having four out of six bounding surfaces free of external forces.

Figs. 16b, d, and f show distributions of the CNP for specimen C at  $\gamma = 0.155$ , 0.1655, and 0.1703, respectively. For shear angles of 0.155 and 0.1655 atoms that become unstable are located close to the bounding surfaces ( $\text{CNP} \sim 20$ ) at two diametrically opposite corners where  $\det(\mathbf{F}^{(i)}) > 1$  locally. The CNP parameter also has the same high value for those atoms on bounding surfaces where no instability was detected. After the occurrence of the global instability, the distribution of unstable atoms correlates well with the distribution in the values of the CNP. No major change in the structure of the system was predicted by the CNP prior to the onset of the global instability. The presence of planes of unstable atoms before the occurrence of the global instability is not observed in the simple shear deformation.

Figs. 17a and b show the distribution of  $\|G\|$  for specimen C at  $\gamma = 0.1655$  and 0.1703, respectively. As for the shear deformations, the maximum value of  $\|G\|$  occurs at points located mainly near the bounding surfaces. From the probability density functions of  $\|G\|$  for strain levels just before and just after the occurrence of the global instability, the expected values are 0.0120 and 0.0948, respectively. Thus  $d\langle\|G\|\rangle/d\gamma$  has a very large value of 17.25 when the global instability occurs.

Fig. 18 shows the evolution with the shear angle of  $d\langle\|G\|\rangle/d\gamma$  and confirms that it is essentially zero till the onset of a global instability when it increases rapidly.



**Fig. 16.** For the simple shear test, distribution of the minimum eigenvalue of the local Hessian and the CNP in system C: (a, b)  $\gamma = 0.1555$ , (c, d)  $\gamma = 0.1655$ , and (e, f)  $\gamma = 0.1703$ .

### 6.2.2. Global instabilities

The variation with the shear angle  $\gamma$  of the system's strain energy density for the shear and the simple shear tests is shown in Fig. 19. In the simple shear deformations, the energy continuously increases up to a point where the global instability occurs. For the shear deformations, slight changes in the curvature of the energy vs. the shear angle  $\gamma$  curve are observed due to the presence of unstable atoms.

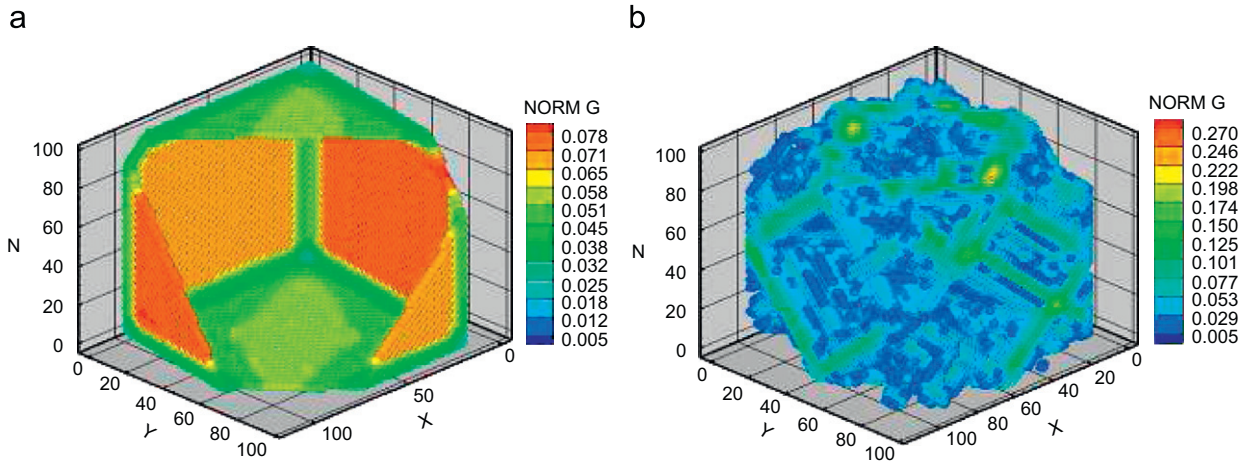


Fig. 17. Distribution of  $\|G\|$  for the simple shear test in system C: (a)  $\gamma = 0.1655$  and (b)  $\gamma = 0.1703$ .

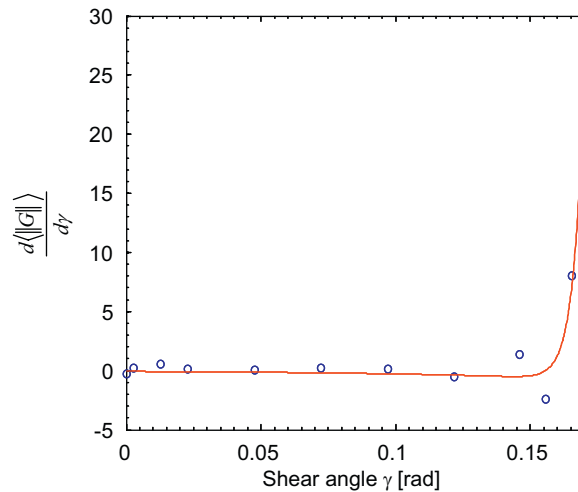


Fig. 18. Derivate with respect to  $\gamma$  of the expected value of  $\|G\|$  for the simple shear test on system C.

For specimens A and B deformed in shear, the energy continuously increases with no major changes in the curvature of the energy vs.  $\gamma$  curve. For specimen C at  $\gamma = 0.0921$ , the presence of two diametrically opposite defects is reflected in a small change of curvature in the energy vs.  $\gamma$  curve. Subsequently, the energy continuously increases till  $\gamma = 0.102$  where a sudden drop in the energy occurs and the system becomes unstable.

Recalling results depicted in Figs. 11 and 15, we conclude that the shear strain at the onset of the global instability equals that at which the percentage of atoms becoming unstable increases the most, and energy of the system drops noticeably.

For the system of Au atoms deformed in simple shear (Fig. 19b), the strain energy density increases monotonically till  $\gamma = 0.1675$  when it suddenly drops by a large amount. For the three specimens, differences among the strain levels at the onset of the global instability are not as pronounced as it is for the shear deformations.

In an attempt to see if the minimum eigenvalue  $\lambda_{\min}^H$  of the Hessian matrix  $\mathbf{H}$  suddenly jumps at the onset of a global instability, we have plotted in Figs. 20a and b the evolution of the change in  $\lambda_{\min}^H$  with respect to  $\gamma$  for the two types of deformations for specimen B. These two plots reveal that indeed  $d\lambda_{\min}^H/d\gamma$  increases noticeably with  $\gamma$  when the system becomes globally unstable. Whereas the evolution with the shear angle of  $d\lambda_{\min}^H/d\gamma$  is oscillatory for shear deformations, it is smooth for the simple shear deformations.

## 7. Conclusions

We have used MM simulations with the TB potential to analyze deformations of three cubes of different sizes comprised of gold atoms deformed in shear and simple shear. In shear, displacements are prescribed of atoms lying on the top and the bottom surfaces of the cube with the other four bounding surfaces kept free of external forces. However, while simulating

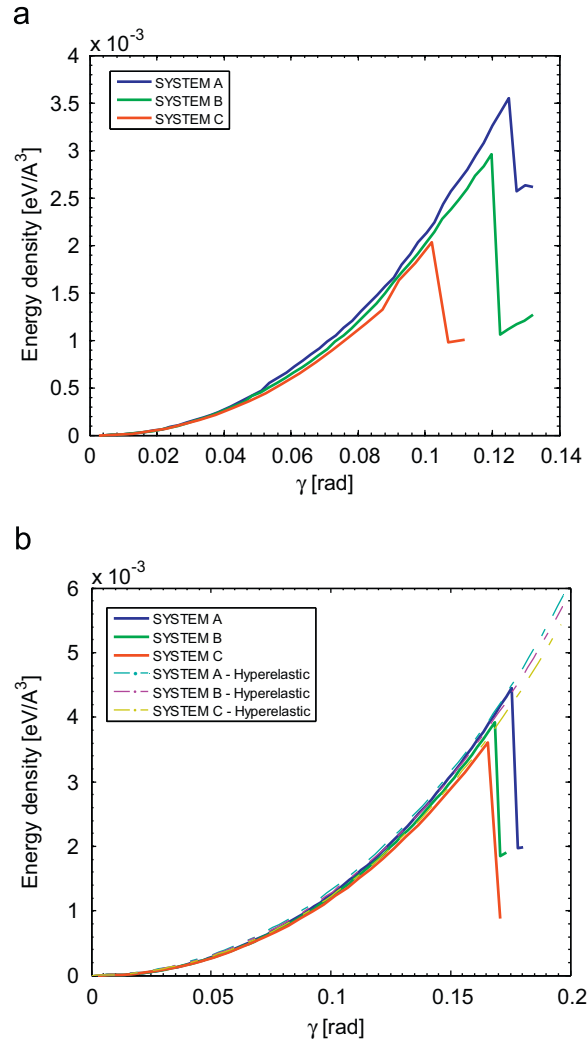


**Fig. 19.** Variation with the shear angle  $\gamma$  of the strain energy density: (a) shear test and (b) simple shear test.

simple shear deformations, displacements are prescribed of atoms on all six bounding planes. Continuum measures of stress and strain are derived from the results of MM simulations. The following four criteria are used to characterize instability at a point: (i) the local atomic acoustic tensor has at least one non-positive eigenvalue, (ii) the minimum eigenvalue of the Hessian of the potential energy of an atom is non-positive, (iii) one or more components of the second-order gradients of displacements becomes very large as compared to its value in the homogeneously deformed regions, and (iv) high values of the CNP. The system is said to be globally unstable when its potential energy ceases to be the minimum in that configuration. Salient results of this work are summarized below.

- Cauchy stresses derived from the following four definitions agree with each other: (i) average of the configurational part of the virial stress tensor, (ii) volume average of the first moments of total forces at atoms on bounding surfaces, (iii) average dipole force tensor, and (iv) the average force per unit area on bounding surfaces.
- For the simple shear deformations, average stresses for an equivalent hyperelastic material with strain energy density derived from the TB potential and the Cauchy–Born rule agree with those computed from the results of the MM simulations.
- Both for the shear and the simple shear deformations normal stresses act on planes where displacements are prescribed, and the specimens exhibit the Poynting effect.
- A discontinuity in the average shear stress vs. the shear angle curve does not imply that the system has become globally unstable; however, a sharp drop in the average shear stress does imply the onset of global instability.

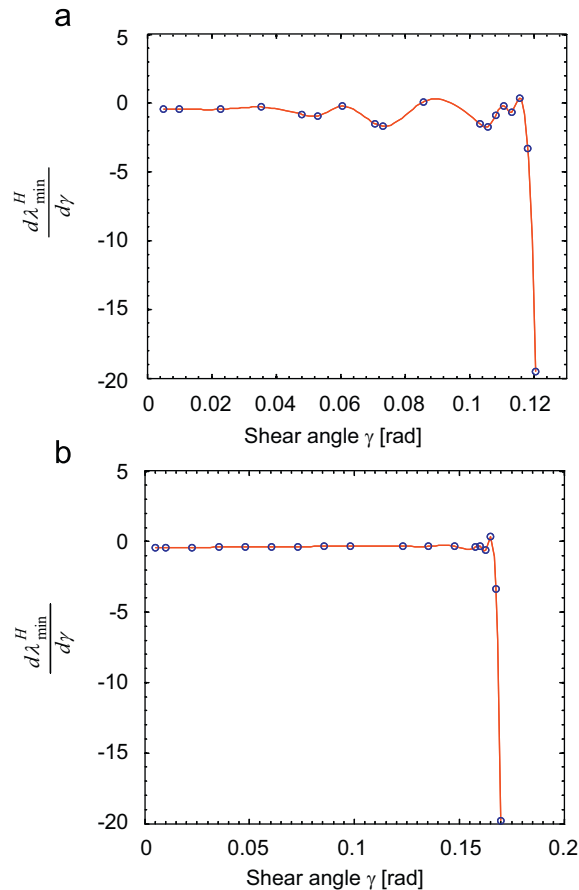


**Fig. 20.** Change of the slope of the minimum eigenvalue of the Hessian matrix  $\mathbf{H}$  with respect to  $\gamma$  for system B: (a) shear test and (b) simple shear test.

- For the shear deformations, the onset of local instabilities precedes significantly that of the global instability. However, for the simple shear deformations the local and the global instabilities occur almost simultaneously.
- The first local instability for the simple shear test occurs nearly at the same shear strain level in the three specimens having widely different number of atoms.
- For the two shear tests studied, the initiation of the local instability is not accurately predicted by a vanishing of an eigenvalue of the local atomic acoustic tensor.
- The occurrence of local instabilities is related with one or more components of the second-order spatial gradients of the displacement becoming very large as compared to their average values in the body.
- The initiation of global instabilities is indicated by the slope of the minimum eigenvalue of the Hessian vs. the shear strain curve becoming very large.

## Acknowledgements

This work was partially supported by the ONR grant N00014-99-06-0567 to Virginia Polytechnic Institute and State University with Dr. Y.D.S. Rajapakse as the program manager, and Virginia Tech's Institute of Critical Technologies and Sciences. AAP was also supported by the COLCIENCIAS – LASPAU scholarship, and the Universidad del Norte in Barranquilla, Colombia. Views expressed herein are those of authors, and neither of the finding agencies nor of their institutions.

## References

- Born, M., Huang, K., 1954. *Dynamical Theory of Crystal Lattices*. Clarendon Press, Oxford.
- Cleri, F., Rosato, V., 1993. Tight-binding potentials for transition metals and alloys. *Phys. Rev. B* 48 (1), 22–33.
- Considerè, M., 1888. *Die Anwendung von Eisen und Stahl bei Konstruktionen*. Gerold-Verlag, Wien.
- Cornier, J., Rickman, J.M., Delph, T.J., 2001. Stress calculation in atomistic simulations of perfect and imperfect solids. *J. Appl. Phys.* 89 (1), 99–104.
- Dimitriev, S.V., Kitamura, T., Li, J., Umeno, Y., Yashiro, K., Yoshikawa, N., 2005. Near-surface lattice instability in 2D fiber and half-space. *Acta Mater.* 53, 1215–1224.

- Ercolessi, F., Parrinello, M., Tosatti, E., 1998. *Philos. Mag.* A 58, 213.
- Ericksen, J.L., 2008. On the Cauchy–Born rule. *Math. Mech. Solids* 13, 199–220.
- Falk, M.L., 1999. Molecular-dynamics study of ductile and brittle fracture in model noncrystalline solids. *Phys. Rev. B* 60, 7062–7070.
- Gullett, P.M., Horstemeyer, M.F., Baskes, M.L., Fang, H., 2008. A deformation gradient tensor and strain tensors for atomistic simulations. *Model. Simul. Mater. Sci. Eng.* 16, 17.
- Hager, W.W., Zhang, H., 2005. A new conjugate gradient method with guaranteed descent and an efficient line search. *SIAM J. Optim.* 16 (1), 170–192.
- Hartley, C.S., Mishin, Y., 2005. Representation of dislocation cores using Nye tensor distributions. *Mater. Sci. Eng. A* 400–401, 18.
- Hill, R., 1962. Acceleration waves in solids. *J. Mech. Phys. Solids* 10, 1–16.
- Ju, S.P., Lin, J.S., Lee, W.J., 2004. A molecular dynamics study of the tensile behavior of ultrathin gold nanowires. *Nanotechnology* 15, 1221–1225.
- Kelchner, C., Plimpton, S., Hamilton, J., 1998. Dislocation nucleation and defect structure during surface indentation. *Phys. Rev. B* 58, 11085.
- Kitamura, T., Umeno, Y., Tsuji, N., 2004a. Analytical evaluation of unstable deformation criterion of atomic structure and its application to nanostructure. *Comput. Mater. Sci.* 29, 499–510.
- Kitamura, T., Umeno, Y., Fushino, R., 2004b. Instability criterion of inhomogeneous atomic system. *Mater. Sci. Eng. A* 379, 229.
- Kouznetsova, V., Geers, M.G.D., Brekelmans, W.A.M., 2002. Multi-scale constitutive modeling of heterogeneous materials with a gradient-enhanced computational homogenization scheme. *Int. J. Numer. Methods Eng.* 54, 1235–1260.
- Lee, W.J., Ju, S.P., Sun, S.J., Weng, M.H., 2006. Dynamical behavior of 7-1 gold nanowires under different axial tensile strains. *Nanotechnology* 17, 3253–3258.
- Li, Q.K., Li, M., 2006. Atomic scale characterization of shear bands in an amorphous metal. *Appl. Phys. Lett.* 88, 241903.
- Lin, J.S., Ju, S.P., Lee, W.J., 2005. Mechanical behavior of gold nanowires with a multishell helical structure. *Phys. Rev. B* 72, 085448.
- Lu, J., Zhang, L., 2006. An atomistic instability condition and applications. *J. Mech. Mater. Struct.* 1 (4), 633–648.
- Miller, R.E., Rodney, D., 2008. On the nonlocal nature of dislocation nucleation during nanoindentation. *J. Mech. Phys. Solids* 56, 1203–1223.
- Mott, P.H., Argon, A.S., Suter, U.W., 1992. The atomic strain tensor. *J. Comput. Phys.* 101, 140–150.
- Ogata, S., Li, J., Hirotsaki, N., Shibutani, Y., Yip, S., 2004. Ideal shear strain of metals and ceramics. *Phys. Rev. B* 70, 104104.
- Pasianot, R., Xie, Z.Y., Farkas, D., Savino, E.J., 1993. Representation of atomistic dislocation core structures. *Scr. Metall. Mater.* 28, 319–324.
- Potirniche, G.P., Horstemeyer, M.F., Wagner, G.J., Gullett, P.M., 2006. A molecular dynamics study of void growth and coalescence in single crystal nickel. *Int. J. Plast.* 22 (2), 257–278.
- Poynting, J.H., 1909. On pressure perpendicular to the shear-planes in finite pure shears, and on the lengthening of loaded wires when twisted. *Proc. R. Soc. Lond. A* 82, 546–549.
- Pu, Q., Leng, Y., Tsetseris, L., Park, H.S., Pantelides, S.T., Cummings, P.T., 2007. Molecular dynamics simulations of stretched gold nanowires: the relative utility of different semiempirical potentials. *J. Chem. Phys.* 126, 144707.
- Rubio-Bollinger, G., Bahn, S.R., Agrait, N., Jacobsen, K.W., Vieira, S., 2001. *Phys. Rev. Lett.* 87, 026101.
- Stakgold, I., 1950. The Cauchy relations in a molecular theory of elasticity. *Quart. Appl. Math.* 8, 169–186.
- Steinmann, P., Elizondo, A., Zunyk, R., 2007. Studies of validity of the Cauchy–Born rule by direct comparison of continuum and atomistic modeling. *Modell. Simul. Mater. Sci. Eng.* 15, S271–S281.
- Truesdell, C., Noll, W., 1992. *The Non-Linear Field Theories of Mechanics*, second ed. Springer, Berlin.
- Tsuzuki, H., Branicio, P.S., Rino, J.P., 2007. Structural characterization of deformed crystals by analysis of common atomic neighborhood. *Comput. Phys. Commun.* 177, 518–523.
- Van Vliet, K.J., Li, J., Zhu, T., Yip, S., Surech, S., 2003. Quantifying the early stages of plasticity through nanoscale simulations and simulations. *Phys. Rev. B* 67, 104105.
- Voter, F., Chen, S.P., 1987. Characterization of defects in materials. In: Siegel, R.W., Weertman, J.R., Sinclair, R. (Eds.), *Mater. Res. Soc. Symp. Proc.*, vol. 82. Materials Research Society, Pittsburgh, p. 175.
- Webb, E.B., Zimmermann, J.A., Seel, S.C., 2008. Reconsideration of continuum thermomechanical quantities in atomic scale simulations. *Math. Mech. Solids* 13, 221–266.
- Zhang, G.M., Batra, R.C., 2004. Modified smoothed particle hydrodynamics method and its application to transient problems. *Comput. Mech.* 34, 137–146.
- Zimmerman, J.A., Kelchner, C.L., Klein, P.A., Hamilton, J.C., Foiles, S.M., 2001. Surface step effects on nanoindentation. *Phys. Rev. Lett.* 87, 165507.